Materials Advances

ROYAL SOCIETY OF CHEMISTRY

PAPER

View Article Online
View Journal | View Issue

Cite this: *Mater. Adv.*, 2025, **6**, 9476

Amoxicillin antibiotic with potential anticancer and antidiabetic activity: acetaldehyde–amoxicillin Schiff base and its vanadyl complex with DFT and docking investigation

Hadeel M. Banbela,[a] Reema H. Aldahiri,[b] Amrajaa S. Abubakr,[c] Magda F. Mohamed[de] and Safaa S. Hassan *[e]

Received 30th May 2025,
Accepted 3rd August 2025

DOI: 10.1039/d5ma00567a

rsc.li/materials-advances

New compounds based on the approved amoxicillin drug were prepared. The new Schiff base ligand (AA) was generated by condensation between the amoxicillin drug and acetaldehyde. The mononuclear VO(II) complex was successfully produced with a molar ratio of 1:2 relative to VO:AA, respectively. Spectroscopic and physicochemical techniques such as elemental analysis, UV-Vis, FT-IR, ^{1}H-NMR, mass spectrometry, molar conductance and magnetic susceptibility were used to characterize the synthesized compounds. Various shifts in the band positions in the FT-IR spectrum of the complex suggested coordination of the VO(II) ion through the azomethinic N and carbonyl O-atoms of the AA ligand. They were moreover analyzed by the TGA thermal technique to confirm the thermal stability of the complex. Furthermore, the compound's formation spontaneity was supported by activation parameters calculated from TGA. Quantum chemical features of both AA and its VO(II) chelate were computed. The AA ligand and its vanadyl chelate revealed comparable anticancer activities against the breast carcinoma (MCF-7) cell line with IC_{50} values of 93.64 ± 0.65 μg mL^{-1} and 97.31 ± 0.55 μg mL^{-1}. Additionally, the antimigration test anticipated that the $[VO(AA)_2]SO_4$ would assist in reducing the metastasis of MCF-7 cells that was suppressed by 46 039 mm over the untreated control at 48 h. The high affinity of the synthesized compounds for DNA binding was explored using electrophoresis with the quantification of the band intensities. The anti-inflammatory effect results indicated that the $[VO(AA)_2]SO_4$ had a slightly higher inhibition percentage than the AA ligand in a concentration-dependent manner. The molecular docking represented the active amino acids interacting with the epidermal growth factor receptor tyrosine kinase. Additionally, the antidiabetic efficacy of the produced compounds was assessed using *in vitro* investigation and molecular docking analyses of α-amylase inhibition. The enzymatic activity of α-amylase progressively diminished with increasing concentrations of the produced AA, VO(II) chelate, and acarbose, achieving maximal inhibitions of 89.9%, 82.8%, and 98.0%, respectively.

Introduction

The World Health Organization (WHO) identifies cancer diseases as the second largest cause of mortality globally. In 2022, there were 2.3 million women diagnosed with breast cancer and 670 000 deaths globally.[1] Every 14 seconds, somewhere in the world, a woman is diagnosed with breast cancer.[2] According to modern cell biology, breast cancer is caused by cell proliferation and migration characterized by an unregulated cell cycle, persistent self-renewal, and generation of cancer stem cells.[3] As our understanding of cancer as a systemic disease has changed, chemotherapy and targeted therapy, which are used to kill cancer cells that have spread to other parts of the body, have taken on a bigger role in the treatment of cancer. The risks to patient care posed by acquired resistance and/or the genotoxic nature of these treatments have also begun to come into sharper focus.[4] Relapses occur in 50% of patients despite radical surgery, and there is no curative therapy for metastatic breast cancer.[5]

Throughout their lives, higher animals, plants, and microbes (such as bacteria, fungi, and actinomycetes) create secondary compounds known as antibiotics that have anti-pathogen or other properties that can impede the growth of other living

[a] *Chemistry Department, College of Applied Science, University of Jeddah, Jeddah, Saudi Arabia*
[b] *Chemistry Department, College of Science, University of Jeddah, Jeddah, Saudi Arabia*
[c] *Department of Chemistry, Faculty of Science, University of Ajdabiya, Ajdabiya, Libya*
[d] *Department of Environmental Science, College of Science, University of Jeddah, Jeddah, Saudi Arabia*
[e] *Department of Chemistry, Faculty of Science, Cairo University, Giza, Egypt. E-mail: hsafaa@sci.cu.edu.eg*

cells.[6] Antibiotics have been shown to decrease cancer development, increase cancer apoptosis, and stop cancer metastases.[7] Adjuvant antibiotics can boost the body's immune system, fight cancer, improve the general state of affairs, increase the effectiveness of therapy, and successfully stop cancer from returning and spreading.[8] One of these promising antibiotics is amoxicillin, which has a variety of biological activities. It is bacteriolytic, containing the β-lactam antibiotic drug of the penicillin class.[9,10] Compared to ampicillin, which efficiently combats germs, amoxicillin's wide range of action is linked to superior oral absorption and higher blood concentrations.[11,12] Schiff base ligands of amoxicillin have been extensively used as a potential bactericidal agent attributable to their role in the treatment of bronchitis, tonsillitis, throat infection, ear infection, typhoid, pneumonia and urinary tract infections.[13] Recent investigations have highlighted the efficacy of the β-lactams: *N*-methylthio β-lactam (A) and *N*-ethylthio β-lactam (B), as depicted in Fig. 1(A) and (B). This novel class of pharmaceuticals has been shown to elicit apoptotic responses in several cancer cell lines, including those from human breast, leukemia, and prostate cancers.[14] Consequently, this class of compounds is extremely useful in the medicinal chemistry field. Amoxicillin (Fig. 1(C)) is regarded as an abortive agent by several medical studies and requires modification, either through alteration of ligand properties or by complexation with metal ions. Antibiotic repurposing can be achieved by metal complexation. It is found that the chelation process improved the biological target of these antibiotics to be used as metal-based drugs for chemotherapy. Metal coordination may also help overcome resistance by protecting the β-lactam ring from enzymatic degradation.[15] Additionally, complexation with vanadium can enhance lipophilicity and membrane permeability, and introduce new mechanisms such as ROS generation or DNA binding, thereby expanding its pharmacological potential beyond traditional antibiotic activity.[16,17] Dipicolinate (dipic)-based vanadium(IV) complexes suppress tumor proliferation by generating reactive oxygen/nitrogen species (ROS/RNS), triggering apoptosis and cell-cycle arrest, and limiting metastasis in various cancer cell lines.[18] In comparison to cisplatin, a new macrocyclic tetranuclear oxidovanadium(V) complex demonstrated greater cytotoxicity against HepG2 liver cancer cells. It disrupted the synthesis of β-tubulin by causing mitochondrial malfunction, ROS-mediated DNA breakage, and cell cycle arrest at the S and G_2/M phases.[19] Given this anticipation, metal complexes of amoxicillin-derived Schiff bases will represent a promising advancement in pharmacological substances for therapeutic applications. Metal ions make a bridge between the drug substances and targeted disease proteins, and thus the field of metal drug interaction chemistry is growing rapidly in the medical and chemical sciences. Our prior research, which involved the condensation of the approved amoxicillin drug with 4-*N*,*N*-dimethylaminobenzaldehyde, followed by chelation with the Pd(II) ion, demonstrated significant efficacy against prostate cancer cells (PC3), yielding an IC_{50} value of 22.6 μg mL^{-1}.[20] Initial studies in the 1980s demonstrated that vanadium compounds could lower blood glucose levels in streptozotocin-induced diabetic rats, paving the way for extensive research into its potential therapeutic applications in type 1 and type 2 diabetes mellitus.[21] Vanadium's capacity to mimic insulin by activating important signaling pathways linked to the insulin receptor is largely responsible for its antidiabetic effects. This mimicry promotes glucose uptake, glycogen synthesis, and the inhibition of hepatic gluconeogenesis.[22,23] In both animal models and clinical trials, a number of vanadium compounds, including sodium metavanadate and vanadyl sulfate, have been demonstrated to have insulin-mimetic and insulin-enhancing properties.[24,25] In order to increase glucose uptake in muscle and adipose tissues, vanadium compounds mechanistically alter important elements of the insulin signaling pathway, such as the inhibition of protein tyrosine phosphatases (PTPs), the activation of the phosphoinositide 3-kinase (PI3K)/Akt pathway, and the enhanced translocation of GLUT4 to the plasma membrane.[26] *In vitro* tests on human colon fibroblasts revealed a synergistic increase in GLUT4-mediated glucose absorption in adipocytes when bis(maltolato)oxidovanadium(IV) or bis(piclinato)oxidovanadium(IV) was mixed with olive leaf polyphenols.[27] David Morales *et al.* reported newly synthesized oxovanadium(IV) pincer complexes that demonstrated normalized lipid and glucose metabolism, alongside potent α-glucosidase inhibition, with IC_{50} values comparable to antidiabetic agent acarbose (*e.g.*, 14–54 μM) in diabetic rats.[28] Despite these encouraging results, vanadium's antidiabetic uses haven't received the same level of attention as its anticancer research. Therefore, vanadium's medicinal relevance must thus be reexamined from a more balanced perspective, one that recognizes its dual potential in the contexts of metabolic disease and oncology.

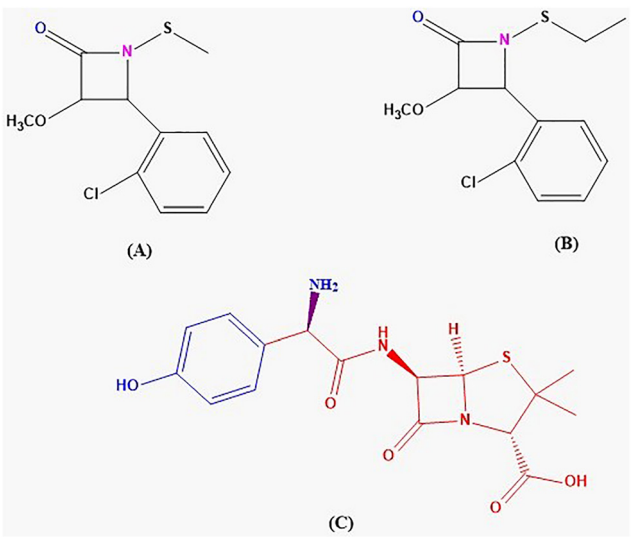

Fig. 1 (A) *N*-Methylthio β-lactam, (B) *N*-ethylthio β-lactams and (C) free amoxicillin.

The goal of this work is to examine the anticancer and antidiabetic potential of the amoxicillin nucleus after its complexation, achieved through the generation of binding centers *via* condensation with a simple aldehyde, such as acetaldehyde, to form a new Schiff base capable of coordinating with the vanadyl ion. Using DNA gel electrophoresis, the new compounds' affinity to bind DNA will be examined. Additionally, the inhibitory impact

of bovine serum albumin (BSA) will be investigated. Molecular docking analysis is recorded to predict the interactions between the protein and the tested compounds.

Experimental part

Materials

Acetaldehyde (99.5% purity), vanadyl sulfate pentahydrate (96% purity), and amoxicillin trihydrate (95% purity) were purchased from Sigma Aldrich in the United States. Every solvent utilized was of the analytical variety.

Preparation of (AA) Schiff base

To make the (AA) Schiff base, 15 mL of methanolic solution containing 1 mmole of acetaldehyde and 25 mL of methanol containing 1 mmole of amoxicillin were mixed. For two hours, the prior mixture was refluxed. After the solution's volume was reduced, a yellowish-orange precipitate formed. After filtering, the precipitate was dried. Ultimately, a 1 : 1 ethanol–water combination was used to recrystallize the precipitate. Thin-layer chromatography (TLC) was employed to evaluate the purity of the synthesized ligand.

$C_{18}H_{21}N_3O_5S$ (AA): color: yellowish-orange; yield: 85.0%.

Calcd.: C, 55.23; H, 5.41; N, 10.73; found: C, 55.02; H, 5.20; N 10.55.

Synthesis of the vanadyl complex

VO(II) chelate was prepared by mixing (AA) ligand (2 mmol in ethanol) and vanadyl sulfate pentahydrate salt (1.0 mmol in ethanol) when exposed to ultrasonic radiation (20 kHz, 150 W). After full addition, the mixture was left in the ultrasonic bath for 60 minutes. The precipitate was washed with a 50% water/ethanol mixture and dried. Scheme 1 represents the synthetic route of AA synthesis and its VO(II) complex.

$C_{38}H_{50}N_6O_{18}S_3V$, $[VO(AA)_2]SO_4{\cdot}3H_2O$: color: yellowish green; yield: 82.0%.

Calcd: C, 43.15; H, 5.03; N, 8.39; found: C, 43.02; H, 4.80; N, 8.00.

Instruments used in analyses

See SI.

Biological screening

The cytotoxicity of the synthesized compounds on breast (MCF-7) cell lines. The MTT assay employing 3-(4,5-dimethylthiazolyl)2,5-diphenyltetrazolium bromide was performed to examine the cytotoxic impact of the evaluated samples.[29] In summary, MCF-7 cells (10^4 cells/100 μL) in complete RPMI (medium/well) were permitted to form a fully developed monolayer sheet overnight, and then were rinsed after 24 hours and exposed to a series of tested materials that were diluted twice, with concentrations ranging from 0 to 250 μg mL^{-1}. The right mass of the material was dissolved in 1 mL of PRMI medium with 2% fetal bovine serum (FBS). From each diluted sample, 100 μL was added to various cultures. Wells were conducted in triplicate with an incubation period of 24 hours in a humidified incubator (37 °C, 5% CO_2). Subsequently, the cells were examined using an inverted microscope to observe the indications of toxicity from the tested sample on the MCF-7 cancer cell line. MTT solution (20 μL of 5 mg mL^{-1} phosphate-buffered saline [PBS]) was administered in every well and the plate was agitated at 150 rpm for 5 minutes with incubation to enable MTT to metabolize and form purple formazan crystals. The formazan crystals were re-dispersed in 200 μL of DMSO while shaking for 5 minutes at 150 rpm. The optical densities (ODs) of the dissolved formazan crystals were measured spectrophotometrically at 560 nm, and background subtraction was done at 620 nm.[30] Outcomes are represented in terms of IC_{50}.

$$\text{Cell viability} = OD_{\text{Treated cells}}/OD_{\text{Untreated cells}} \times 100$$

In vitro scratch wound healing assay

The scratch assay was employed to assess the wound–healing effects of VO(II) chelate on MCF-7 cells.[29] In summary, the cells were transferred into six-well culture plates until they achieved a confluence of 80.0–90.0%. Next, a sterile 200-μL pipette tip was utilized to scrape the cell monolayers in each well, which was followed by several rinses with PBS. Subsequently, the cells received treatment with 93.64 μg mL^{-1} VO(II) chelate. Subsequently, at 0 and 48 hours of incubation, the inverted light microscope was utilized to observe and record the progression of wound closure. The rate of migration was determined in the following manner:

$$\text{Rate of migration (RM)} = w_i - w_f/t$$

where w_i represents the average initial wound width (μm), w_f denotes the average final wound width (μm), and t is the duration of the test in hours.

CT-DNA binding

See SI.

Alpha-amylase inhibition

The 3,5-dinitrosalicylic acid (DNSA) technique was used to perform the α-amylase inhibition experiment.[31] To achieve concentrations ranging from 1.9 to 1000 μg mL^{-1}, each synthesized molecule was first diluted in a minimum volume of 10% DMSO, followed by a dilution in buffer (Na_2HPO_4/NaH_2PO_4) (0.02 M), and NaCl (0.006 M) at pH 6.9. Following a 10-minute incubation period at 30 °C, 200 μL of the sample and 200 μL of α-amylase solution (2 units per mL) were combined. 200 μL of the starch solution (1% in water (w/v)) was then added to each tube, and the tubes were incubated for three minutes. The reaction was stopped by adding 200 μL of DNSA reagent, which is composed of 20 mL of a 96 mM solution of 3,5-dinitrosalicylic acid and 12 g of sodium potassium tartrate tetrahydrate in 8 mL of 2 M NaOH. The solution was thereafter heated for 10 minutes at 85–90 °C in a water bath. Upon reaching room temperature, it was diluted with 5 mL of distilled water, and the absorbance was measured at 540 nm using a UV-visible biosystem 310 spectrophotometer. The 100% control with full enzyme activity was established by replacing the tested sample with 200 μL of buffer. A control reaction was established for each sample at every concentration, excluding the enzyme solution. The α-amylase inhibitory activity was

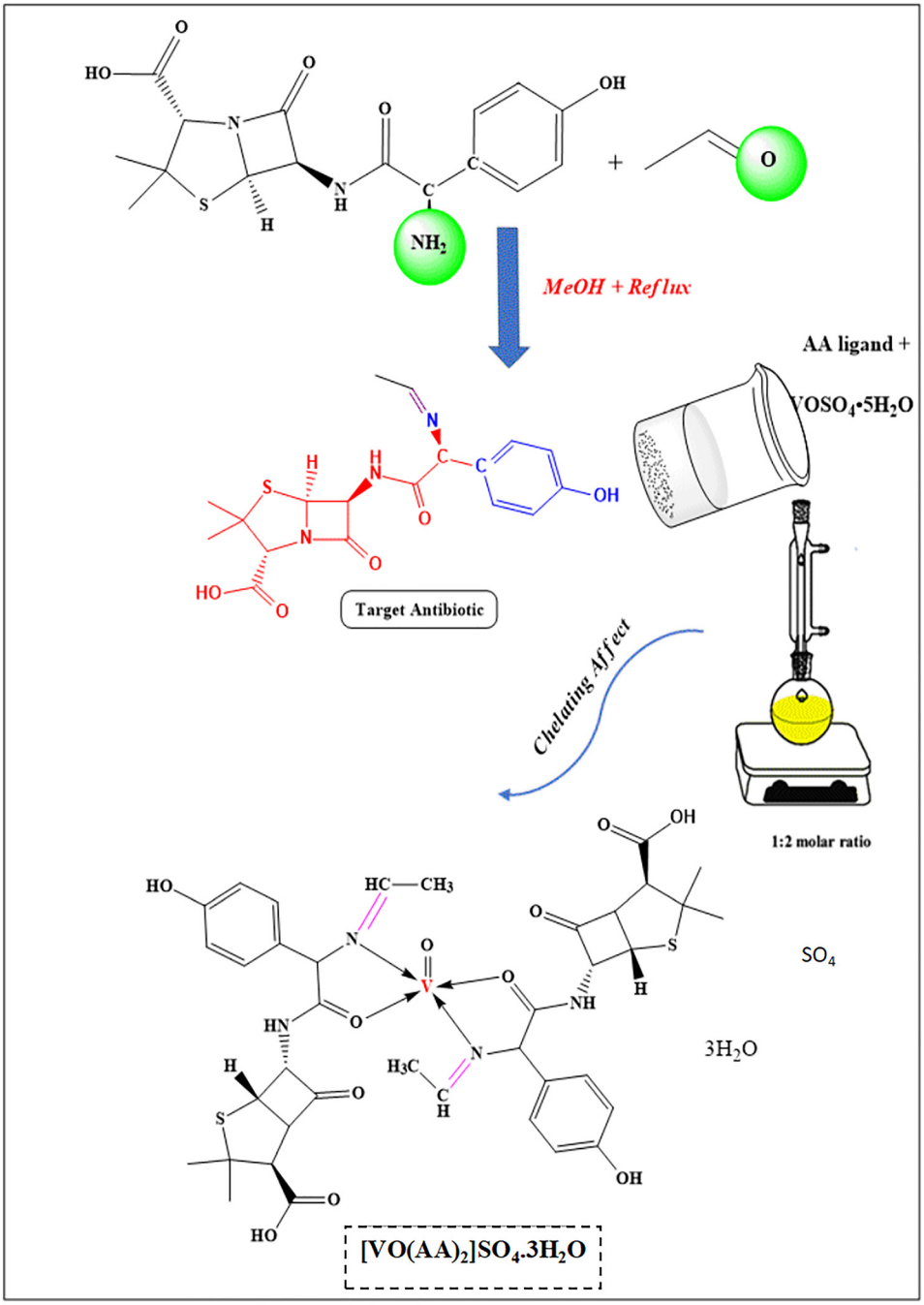

Scheme 1 Synthetic route of the amoxicillin–acetaldehyde Schiff base (AA) and its $[VO(AA)_2]SO_4$ complex.

expressed as percent inhibition, computed using the equation presented below: the % α-amylase inhibition was graphed against the sample concentration, and the IC_{50} values were derived from the graph.

$$\%\ \alpha\ \text{amylase inhibition} = 100 \times (\text{Abs}_{100\%\ \text{control}} - \text{Abs}_{\text{Sample}})/\text{Abs}_{100\%\ \text{control}}$$

Bovine serum albumin denaturation inhibition measurement

See SI.[32]

Computational methods

See SI.[33–35]

Results and discussion

Compound's structure description

As shown in Table 1, the elemental analysis demonstrates that the VO(II)-complex was produced in a molar ratio of 1 : 2 with respect to AA and VO(II), respectively.

Table 1 Physical characterization, and analytical results of the free AA ligand and its VO(II) complex

Compound	Formula (M. wt)	Color	Yield %	Found (calc.)%		
				C	H	N
AA ligand	$C_{18}H_{21}N_3O_5S$ (391.44)	Yellowish-orange	85%	55.02 (55.23)	5.20 (5.41)	10.55 (10.73)
VO(II) complex	$C_{36}H_{50}N_6O_{18}S_3V$ (1001.95)	Yellowish-green	82%	43.02 (43.15)	4.80 (5.03)	8.00 (8.39)

Fig. S1a and b show the FT-IR spectra of the AA ligand and its VO(II) chelate. The peak shifting observations are a key method for inspecting the binding coordination mechanism of the metal chelates using vibrational frequency analysis.[29,36–39] Frequencies assigned to aromatic nucleus C=C, ν_{NH}, amidic $\nu_{C=O}$, β-lactamic C=O ($\nu_{C=O}$), and carboxylate ($\nu_{as}COO^-$) (ν_sCOO^-) have all been identified at 1519, 3510, 1689, 1550 and 1381 cm^{-1},[40] respectively, in the uncomplexed AA as described in Table 2. These results are in accordance with the literature.[41–43] A new absorption band at 1666 cm^{-1} was observed in the AA chart and is related to the ν(C=N) stretching vibration overlapping with the ν(C=O) amidic section, which is consistent with the designated values of the 1660 cm^{-1} region in supplementary work.[44,45] According to Hooke's rule, the electron density near the prominent functional groups may rise or fall depending on how the metal binds to the ligand.[46] Therefore, following cooperation with vanadyl salt, this might display a lower or greater vibrational energy. This was observed because the vanadyl center pulls electrons inductively from the imine nitrogen and carbonyl oxygen. Furthermore, the energy shift in this absorption band confirms the contribution of the azomethinic N-atom and carbonyl O-atom in complexation with the VO(II) ion.[47–49] A broad band with an absorption maximum of 3510 cm^{-1} in the spectrum of the ligand is possibly due to the collapse of N–H and O–H stretching peaks.[50] The position of this band, however, remains practically unaltered in the prepared VO(II) complex, indicating non-involvement of the imino nitrogen atom in coordination with the VO^{2+}.[51] The spectra of the complex revealed a broad band around 3479 cm^{-1}, which is assigned to hydrated water molecules $\nu(H_2O)$.[52–56] The bending vibration of the hydrated water molecule in the outer sphere area is responsible for the less strong infrared band at 616 cm^{-1}. The absorption bands at 970 cm^{-1} in the vanadyl complex have been observed, and these bands can be attributed to the ν(V=O) vibration. This finding is consistent with previous reports describing this vibration.[29,57] The discovery of additional bands in the lower frequency regions at 425 and 532 cm^{-1} correspond to (V–N) and (V–O) stretching vibrations that are absent in the AA ligand's infrared spectrum. It further supports the chelation process of the VO(II) metal ion.

NMR observations in DMSO-d_6 as a solvent: the ^{1}H-NMR spectrum of the synthesized AA presented all the predictable protons as depicted in Fig. S2. The ^{1}H NMR spectrum of the amoxicillin ligand based on condensation with acetaldehyde detected an extremely de-shielded singlet at a low-field area δ = 8.50 ppm attributed to the proton of the azomethinic δ (H–C=N) portion, in conformity with the reported values of δ = 8.36 ppm in previous investigations by Wasfi Abood Al-Masoudi.[58] In the lower-field region of the spectrum (δ = 6.63–7.30 ppm), distinct sets of signals can be observed. These signals can be attributed to the protons found in the aromatic constituents, specifically the benzene ring protons. In addition to the peaks given by δ (CO–CH) and δ (N–CH) on the β-lactam ring, they seemed to be at δ = 4.6, 4.7 and δ = 8.10 ppm, respectively,[59,60] in agreement with the reported values of δ = 4.81, 3.83 and δ = 8.20 ppm in similar earlier works.[59–63] It is worth noting that the protons of Ar–OH resonate as a singlet at δ = 5.15 and 4.83 ppm.[60] A single peak attributed to the hydroxyl group of carboxylic acid appeared at δ = 9.85 ppm,[64] in agreement with the reported value of δ = 9.42 ppm in earlier research investigations,[60] as well as signal peaks at (δ = 2.50, 3.70, 1.08, and 3.19 ppm) attributed to δ solvent DMSO, the δ(–CH) proton of the amoxicillin skeleton, and the δ(–CH_3) protons of the acetaldehyde fragment, respectively. The chemical shifts of ^{1}H NMR are listed and assigned in Table 3.

The electronic spectrum of the ligand (AA) presents two absorption bands at 279 and 361 nm attributed to $\pi \rightarrow \pi^*$ (aromatic ring) and $n \rightarrow \pi^*$ (C=O and C=N), respectively.[65] These transitions were shifted in the chelate at (280–357) for the VO(II) complex. The shift is ascribed to the complexation properties of the ligand to the VO(II) ion.[66] The solution of the vanadyl complex exhibits a distinct absorption peak at λ_{max} 357 nm, which is attributed to the AA ligand-to-metal charge transfer (LMCT) transition. Moreover, the visible spectrum shows a peak at λ_{max} 740 nm (13 513 cm^{-1}), corresponding to the $2B_2 \rightarrow 2E$ transition.[36] These findings are consistent with previous research at 13 280 cm^{-1} and confirm the square pyramidal geometry of the oxovanadium(II) complex[67] that is supported by the magnetic moment value of 1.79 B.M. due to one unpaired electron.[66] Fig. 2 observes the mentioned transitions of the AA ligand and its VO(II) chelate.

The VO(II) chelate was tested at pH 3, 7, and 11 at room temperature. It showed low stability in both acidic and basic media, with rapid degradation and precipitate formation in the basic conditions. In contrast, the complex remained stable with minimal degradation at neutral pH (7), indicating that neutral conditions favor its stability.

The thermal stability data of the VO(II) complex indicated the subsequent degradation processes as illustrated in Fig. 3(a) and Table 4. The VO(II) complex decomposes mainly in three steps. The first step is attributed to the loss of three hydrated water molecules from the outer sphere of the crystalline solid (dehydration) and SO_3 with a mass loss of (obs. = 14.0%, calc. = 13.43%). The decomposition of the coordinated organic ligand was decomposed through three fast steps with a total mass loss of (obs. = 81.12%, calc. = 81.46%) leaving behind vanadium metal with a residual mass (obs. = 4.88%, calc. = 5.10%) that is compatible with Al-Wasidi *et al.*[68]

Table 2 The most important experimental and theoretical vibrational frequencies (cm^{-1}) for the ligand and its VO(II) complex

	Overlapping of ν(C=N) imine & $\nu_{C=O}$ + ν(C=C) aromatic		$\nu_{C=O}$ (β-lactamic)		δ_{NH} (amide) + O–H moiety		$\nu_{as}COO^-$		$\nu_{s}COO^-$		ν(M–N)		ν(M–O)	
Compound	DFT	Exp.	DFT	Exp.	DFT	Exp.	DFT	Exp.	DFT	Exp.	DFT	Exp.	DFT	Exp.
AA	1669, 1525	1666, 1519	1696	1689	3525	3510	1552	1550	1390	1381	—		—	—
VO(II) complex	1651, 1516	1630, 1512	1696	1689	3526	3510	1522	1519	1438	1433	427	425	544	532

Table 3 Analysis of the ^{1}H-NMR spectrum of the AA ligand experimentally and theoretically

	Ar–OH + hydroxyl group of carboxylic		Aromatic ring protons		H–C=N Protons		δ(NH sec.) amide		δ(CO–CH) and δ(N–CH)		δ(CH–S) skeleton		$-CH_3$ protons of amoxicillin + CH and $-CH_3$ protons of acetaldehyde	
Compound	DFT	Exp.	DFT	Exp.	DFT	Exp.	DFT	Exp.	DFT	Exp.	DFT	Exp.	DFT	Exp.
Ligand, AA	4.50–4.95	4.83–5.15, +9.85	6.25–6.80	6.63–7.30	8.20	8.50	7.80	8.10	3.60, 4.00	4.60, 4.70	3.20	3.39	1.20, 1.50 + 2.90, 0.95	1.27,1.55 + 3.70, 1.08 and 3.19

Utilizing the Coats–Redfern (CR) and Horowitz–Metzger techniques, the thermodynamic parameters (ΔE, ΔH, ΔS, and ΔG) were assessed,[69] as seen in Fig. 3(b) and (c) and summarized in Table 4. The stability of the VO(II) chelate under investigation may be connected to the high activation energy (E^*) values. The minor positive values of the activation entropies ΔS^* might suggest a little alteration in the ordered state of the reactants and activated molecules.[70] The positive number indicates a rise in disorder during the response, despite the slight shift. The processes are not spontaneous, as indicated by the positive values of ΔG^*. This suggests that the processes need an energy input to continue and are not spontaneously favored.

Mass spectral evaluation and the proposed fragmentation of the AA ligand and its VO(II) chelate are observed in Fig. 4(a) and Table 5. The spectrum of AA displays a molecular ion peak at m/z = 390 (17.00%), which is equivalent to $[M^+ + 1]$ and corresponds to ligand fraction [($C_{18}H_{21}N_3O_5S$) atomic mass 391.44]. The charged organic ligand without the β-lactamic oxygen was thought to be the source of the second strong signal at 183.02 m/z, given the probable fragments. Moreover, the spectrum demonstrates imperative fragments at m/z = 107.87 $[C_5H_2NS]^+$ and 46.57 $[CH_2S]^+$. A proposed degradation pathway of free AA is displayed in Scheme S2. The molecular ion peak for the VO(II) complex was observed at m/z = 998.60 (23.73%), as seen in Fig. 4(b). Besides, the spectrum displays miscellaneous fragments at m/z = 997.55 $[C_{36}H_{49}N_6O_{18}S_3V]^+$, 937.03 $[C_{34}H_{45}N_6O_{18}S_2V]^+$, 666.68 $[C_{26}H_{31}N_6O_{10}SV]^+$, 545.33 $[C_{18}H_{22}N_6O_9SV]^+$, 360.61 $[C_{11}H_{15}N_5O_6V]^+$, 152.85 $[C_7H_{10}NO_3]^+$, 100.88 $[C_7H_6N]^+$ and 74.77 $[C_5H_6N]^+$, corresponding to the removal of a proton, C_2H_4S, $C_8H_{14}O_8S$, C_8H_9O, $C_7H_7NO_3S$, $C_4H_5N_4O_3V$, O_3H_4, and two carbon atoms from the $[C_{36}H_{50}N_6O_{18}S_3V]$ moiety. A proposed degradation pathway of the free VO(II) complex is displayed in Scheme S3. The molecular weight, as seen in Fig. 4(b), exceeds 1000 amu, confirming the proposed structure. The mass spectra of the AA ligand and its VO(II) chelate show good agreement with the investigated previous techniques, confirming the postulated molecular formula (Scheme 1).

DFT study

The optimized structures of the AA ligand and its vanadyl chelate are pointed out in Fig. 5 with estimated bond lengths and angles in Table 6. The bond lengths of the AA ligand are changed after its coordination to the VO(II) ion, especially the bonds related to the donor sites. Some bonds experience elongation [(C10–N11), (C12–O22), (C13–N14) & (C14–C26)] and contraction [(C12–C13) & (C26–C27)] in order to attain

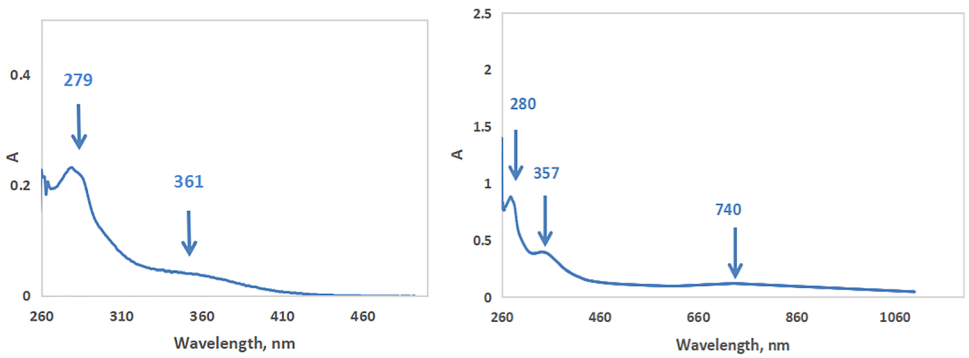

Fig. 2 Electronic transitions of the AA ligand and its $[VO(AA)_2]SO_4$ chelate, respectively.

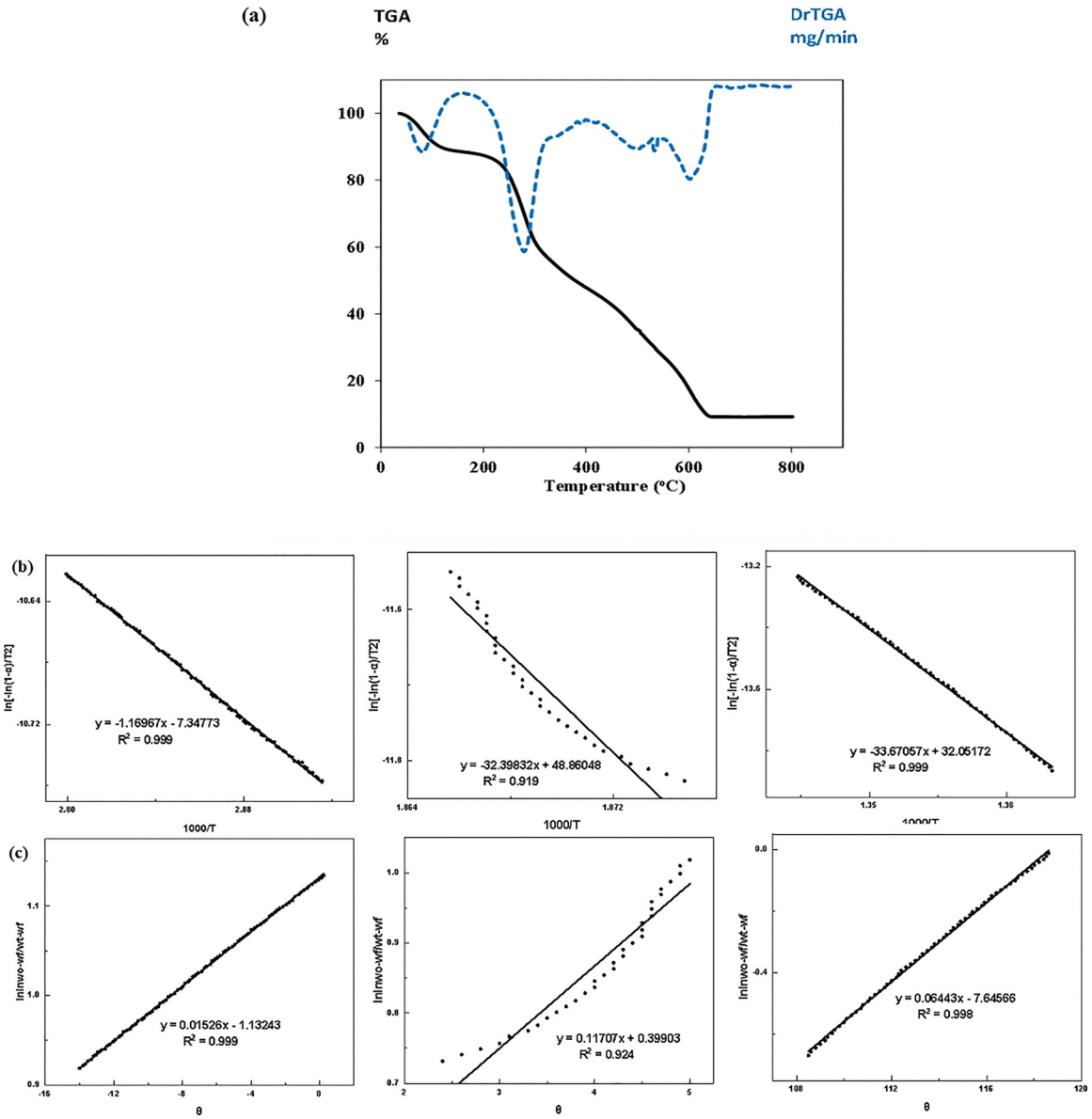

Fig. 3 (a) TG curve of $[VO(AA)_2]SO_4{\cdot}3H_2O$ chelate, and (b and c) Coats–Redfern and Horowitz–Metzger plots for the decomposition steps, respectively.

Table 4 Activation parameters for the decomposition of the $[VO(AA)_2]SO_4{\cdot}3H_2O$, determined using the Coats–Redfern and Horowitz–Metzger methods

Compound	Step	r^2	E^* (kJ mol^{-1})	ΔH^* (kJ mol^{-1})	ΔS^* (kJ mol^{-1} K^{-1})	ΔG^* (kJ mol^{-1})
VO(II) chelate	1st	0.999	9.72	676	−0.22	88.73
		0.989	16.17	13.20	−0.21	90.58
	2nd	0.919	269.36	264.94	0.26	125.82
		0.924	274.43	270.01	0.26	127.49
	3rd	0.999	279.94	274.74	0.12	198.97
		0.998	209.24	204.05	0.08	154.0

r^2: Correlation coefficient.

the intended coordination structure. After coordination, new bonds are formed between the carbonyl oxygen and N of the imine group with the VO(II) ion. Changes in the values of the chelation surrounding angles were observed as [(C10–N11–C12), (N11–C12–O22), and (C12–N13–N14)]. These changes resulted due to the bonding during complex creation. The

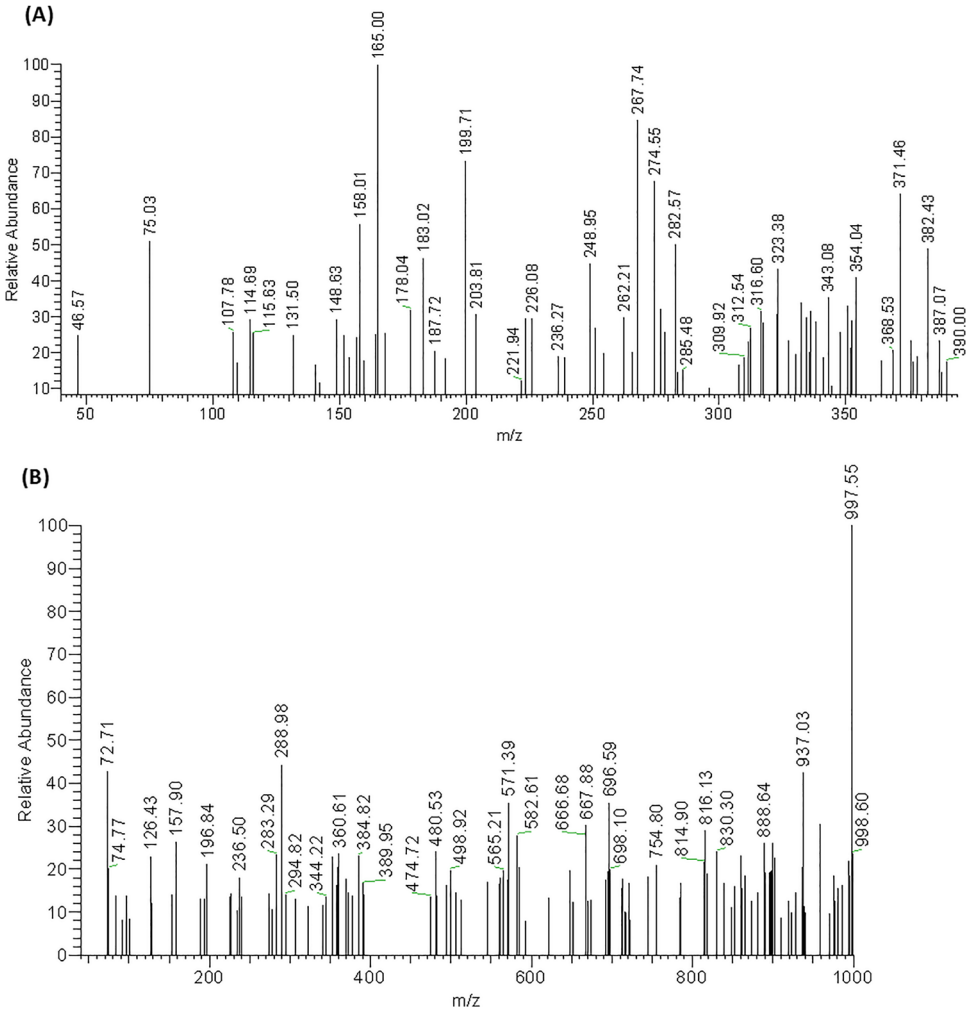

Fig. 4 (A) Mass spectra of the AA ligand, and (B) $[VO(AA)_2]SO_4{\cdot}3H_2O$ chelate.

Table 5 Mass spectral fragmentations of the ligand (AA) and its VO(II)-AA chelate

Compound	Fragmented ion	m/z^+ values		Relative abundance (%)	Missing species
		Calc.	Found		
AA ligand	$[C_{18}H_{21}N_3O_5S]$	391.44	390.00	17.00	—
	$[C_8H_{10}NO_3S]^+$	199.00	199.71	73.28	$C_{10}H_{11}N_2O_2$
	$[C_8H_{10}NO_2S]^+$	183.71	183.02	46.37	O
	$[C_5H_2NS]^+$	107.02	107.87	25.90	$C_3H_8O_2$
	$[CH_2S]^+$	45.87	46.57	24.87	C_4N
VO(II) complex	$[C_{36}H_{50}N_6O_{18}S_3V]$	1001.95	998.60	23.73	—
	$[C_{36}H_{49}N_6O_{18}S_3V]^+$	997.60	997.55	100	H
	$[C_{34}H_{45}N_6O_{18}S_2V]^+$	937.49	937.03	42.63	C_2H_4S
	$[C_{26}H_{31}N_6O_{10}SV]^+$	666.97	666.68	27.82	$C_8H_{14}O_8S$
	$[C_{18}H_{22}N_6O_9SV]^+$	545.68	545.33	17.18	C_8H_9O
	$[C_{11}H_{15}N_5O_6V]^+$	360.27	360.61	23.63	$C_7H_7NO_3S$
	$[C_7H_{10}NO_3]^+$	152.67	152.85	14.09	$C_4H_5N_4O_3V$
	$[C_7H_6N]^+$	100.85	100.88	8.54	$O_3H_4C_2$
	$[C_5H_6N]^+$	76.88	74.77	20.22	

metal electron density was increased after chelation to become +0.956 due to AA ligand to V charge transfer. Certain structural reactive sites were identified by the molecular electrostatic potential (MEP) study. Atoms possessing a positive electrostatic potential can adhere to the sphere of negative electrostatic potential, serving as active sites for the coordination of vanadium ions. Overall, the vanadyl complex under investigation showed negative regions on their coordination centers (N14 & O22) and

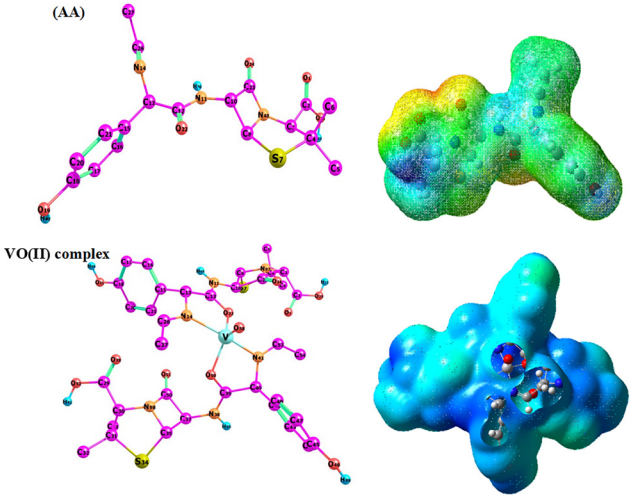

Fig. 5 Geometric structure and MEP of the AA ligand and its $[VO(AA)_2]SO_4$, respectively.

positive electrostatic potential maps on their skeleton, which increased their biological activity.[71] The energy value of the synthesized vanadyl complex was assessed utilizing density functional theory (DFT),[72] including several characteristics including dipole moment, hardness (η), softness (S), energy gap, chemical potential (μ), and electronegativity (χ), as shown in Table 7. The frontier molecular orbitals (FMO) are explored in Fig. 6. The DFT analysis revealed that the VO(II) chelate demonstrated greater negative values than the initial AA ligand, signifying the chelation process. The previous parameters were calculated using the following equations:

$$\eta = \frac{(I-A)}{2}, \quad S\frac{1}{2\eta}, \quad \mu = \frac{-(I+A)}{2}, \quad \chi = \frac{(I+A)}{2}$$

Based on the HOMO–LUMO energy gap, the VO(II) chelate was shown to be a softer molecule compared to its parent AA ligand. A reduced gap signifies a softer molecule, with the HOMO and LUMO denoting the frontier molecular orbitals, as seen in Fig. 7. The ability to receive electrons is referred to as softness, whereas its opposite is termed hardness.[73] The energy required to remove an electron is characterized by the ionization potential, equivalent to the energy of the highest occupied molecular orbital (HOMO), whereas the energy of the lowest unoccupied molecular orbital (LUMO) corresponds to the electron affinity, which releases energy upon the addition of an extra electron to the system.[29] The significant energy disparity between the HOMO–LUMO energy values of the AA ligand and its chelate[74] demonstrates the stability of the molecules. Also, E_{HOMO} of AA ligand < VO(II) chelate. Thus, we may assert that AA possesses a greater capacity to transfer its HOMO electron to the electron-accepting species. However, the VO(II) complex exhibits greater sensitivity to receive electrons from electron-rich species. The polarity of the AA ligand diminishes upon interacting with the VO(II) ion, as shown by the magnitude of their dipole moments.[36] Following chelation, the FMO orbital electron clouds spread out across the aromatic portion of the AA ligand and expand to include the metal's coordination center.

Table 7 Ground state properties of the AA ligand and its VO(II) chelate using B3LYP/6-311G and B3LYP/LANL2DZ, respectively

Parameter	AA	VO(II) complex
E_T, Hartree	−1637.01	−2643.90
E_{HOMO}, eV	−6.69	−10.75
E_{LUMO}, eV	−1.26	−7.23
ΔE, eV	5.42	3.51
$I = -E_{HOMO}$, eV	6.69	10.75
$A = -E_{LUMO}$, eV	1.26	7.23
χ, eV	3.98	8.99
η, eV	2.71	1.75
S, eV^{-1}	0.18	0.56
μ, eV	−3.98	−8.99
Dipole moment (Debye)	5.44	2.92

Theoretical IR spectroscopy observations

The computation of the FT-IR investigations for the compounds under study was carried out, which provides a comparison between theoretical and experimental results. As observed in Table 2 and Fig. S1, there is a complete agreement and matching between the simulated peak characteristics for the AA ligand and its VO(II) chelate with the experimental data. The accuracy of theoretical FTIR frequencies is often assessed using the Mean Absolute Error (MAE), with values below 10 cm^{-1} considered excellent.[75] In our study, the MAE values were 7 and 8.75 cm^{-1} for AA and its vanadyl chelate, respectively, indicating strong agreement with experimental data and confirming the reliability of the theoretical model.

Theoretical NMR. Theoretical ^{1}H-NMR signals have been detected as seen in Table 3 and Fig. S2. The mean absolute

Table 6 Some of the optimized bond lengths, Å and bond angles, degrees, for the AA ligand and its VO(II) chelate using B3LYP/6-311G and B3LYP/LANL2DZ, respectively

Bond length (Å)	AA	VO(II)-complex	Bond angles	AA	VO(II)-AA
R(C10–N11)	1.44044	1.46837	A(C10–N11–C12)	121.580	119.474
R(N11–C12)	1.37137	1.33028	A(N11–C12–O22)	122.202	118.841
R(C12–O22)	1.21428	1.29851	A(C22–C12–C13)	123.566	118.107
R(C12–C13)	1.54768	1.52786	A(C12–C13–N14)	108.506	104.545
R(C13–N14)	1.45870	1.51904	A(C13–N14–C26)	117.855	118.243
R(C14–C26)	1.26626	1.30109	A(O50–N14–O22)	—	75.352
R(C26–C27)	1.49677	1.48990	A(O50–O58–N14)	—	62.533
R(O14–V)	—	2.11330	A(O58–V–N14)	—	100.783
R(O22–V)	—	1.94909			
R(O58–V)	—	1.58317			

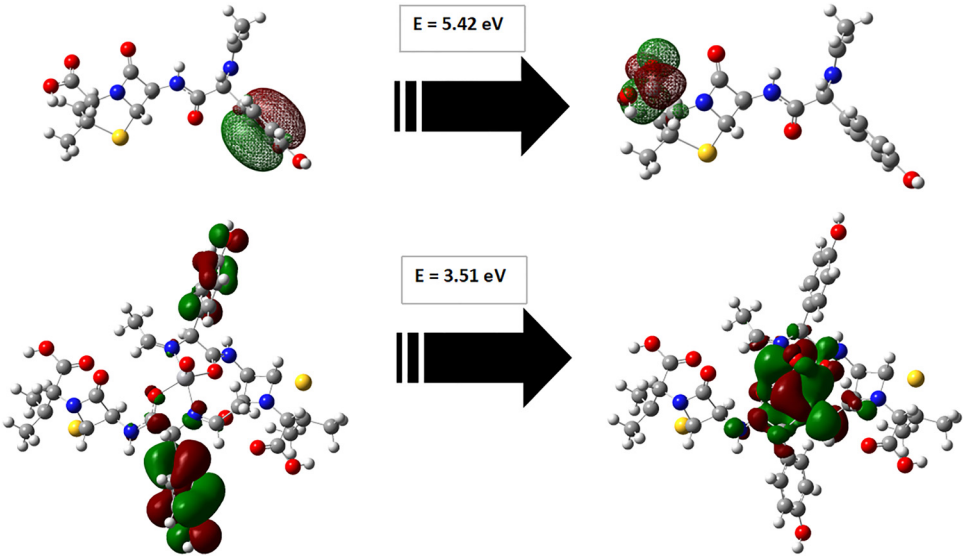

Fig. 6 FMO of the AA ligand and $[VO(AA)_2]SO_4$.

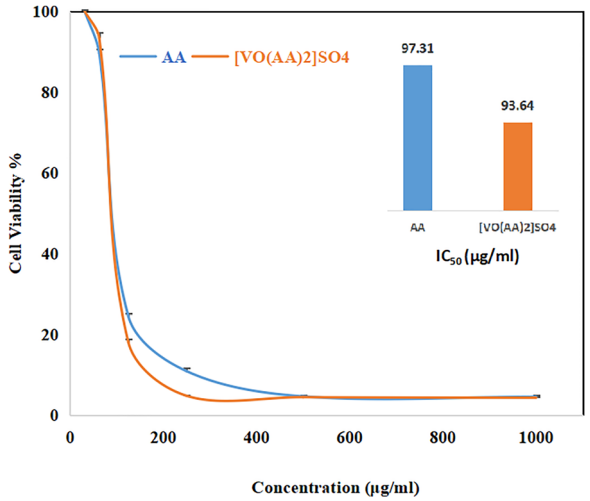

Fig. 7 An MTT assay demonstrated a remarkable reduction in the breast cancer cell line (MCF-7) after being treated for 24 h with various concentrations of (AA &$[VO(AA)_2]SO_4$) and the inset plot represents their IC_{50} values.

error (MAE) values typically range from 0.2 to 0.5 ppm for well-optimized geometries.[76] In our case, the calculated mean absolute error (MAE) is 0.38 ppm, indicating a good agreement between theoretical and experimental chemical shifts.

Measurement of cytotoxicity on MCF-7 cells with molecular docking

It was favored to use one of the approved and cost-effective drugs in the treatment of one of the most severe diseases, breast cancer, which is one of the female malignancy cancer types. The modified amoxicillin drug (AA) was tested, along with its VO(II) chelate against the MCF-7 cancer cell line using different concentrations. The proportions of growth inhibition and remnant viable cells are depicted in Fig. 7. The cell line cytotoxicity was found to be in a concentration-dependent manner for both compounds and the viability of cancer cells was dramatically decreased with increasing the concentrations of AA and $[VO(AA)_2]SO_4$. In addition, based on the 50% inhibitory concentration values (IC_{50}), the chelation process improved the inhibition of breast cancer cell growth relative to the parent ligand. The $[VO(AA)_2]SO_4$ and AA ligand exhibited IC_{50} values of 93.64 ± 0.65 µg mL^{-1} and 97.31 ± 0.55 µg mL^{-1}, respectively, which may be attributed to the ability of AA to generate reactive oxygen species (ROS), disrupt mitochondrial function, and interact with DNA, as previously reported for VO(II) complexes by Manuel *et al.*[77]. Additionally, this improvement may result from the coordinated ligand's increased acidity toward the metal ion because the metal's positive charge creates stronger hydrogen bonds, which boost biological activity. Vanadyl activity may be related to the variable oxidation states that can increase the probability of interactions between the complex and protein constituents. The chelation process reduces the polarity of metal atoms by partly sharing their positive charge with donor groups and potential π electron delocalization in the chelation rings. The chelation procedure enhances the hydrophobic qualities of the central atoms, promoting their penetration through cancer cells. The way it works might include forming hydrogen bonds *via* the azomethine nitrogen atom with the cell components' active sites, which can disrupt the regular cell functions.[74] However, the small change between the IC_{50} values between the ligand and its vanadyl chelate indicates that the activity is mainly due to the amoxicillin moiety. Therefore, we can say that the amoxicillin moiety can be used as an anticancer drug against the MCF-7 breast cell line. The anticancer activity improved following coordination. The vanadyl complex exhibited low toxicity toward normal cells, as evidenced by its high IC_{50} value of 238.03 ± 2.77 µg mL^{-1} against the WI-38 cell line, as shown in Fig. S3. The IC_{50} values for cisplatin in MCF-7 cells

have been reported as 4 μg mL^{-1}, while their resistant derivative, MCF-7/DDP, showed an IC_{50} of around 15 μg mL^{-1}.[78] Although our compounds exhibit relatively high IC_{50} values of 93 and 98 μg mL^{-1} against MCF-7 breast cancer cells, they remain valuable candidates due to the well-established resistance of MCF-7 cells to cisplatin and the drug's serious side effects, such as kidney and nerve toxicity.[79] Doxorubicin demonstrated the most effective anticancer potential against MCF-7 breast cancer cells, as reported by Qiu Hong Fan *et al.*,[80] with a low IC_{50} value of 0.68 ± 0.04 μg mL^{-1}. The lower activity of the vanadyl complex compared to doxorubicin may be due to its bulkier structure, which can hinder membrane permeability and cellular uptake. This bulkiness may also reduce its binding affinity to essential intracellular targets, leading to decreased cytotoxic efficacy. However, despite their reduced activity, our compounds offer a significant advantage in terms of cost-effectiveness and accessibility, making them promising candidates for further development. Notably, our compounds are based on amoxicillin—a widely used, FDA-approved β-lactam antibiotic known for its safety and affordability—providing a favorable foundation for further modification.[81] A comparison between the anticancer results and our previously reported research studies of approved drugs revealed similar behavior with the metformin Schiff base with different metal ions, such as Pd(II), Pt(II) and VO(II). All compounds exhibited $IC_{50} > 50$ μg mL^{-1} against breast cancer[82] but the VO(II) chelate revealed a better IC_{50} of 25 μg mL^{-1} based on the Schiff base formed between 4-(diethylamino)benzaldehyde and metformin.[83] Additionally, the condensation of the approved amoxicillin drug with 4-*N*,*N*-dimethylaminobenzaldehyde, followed by chelation with the Pd(II) ion, demonstrated significant efficacy against prostate cancer cells (PC3), yielding an IC_{50} value of 22.6 μg mL^{-1} [20] that revealed the potential activity of metal complexes of amoxicillin-based complexes against different cancer cell lines. The morphological alterations of treated cells were visualized under an inverted microscope as shown in Fig. 8. The most visualized apoptotic features due to AA and its VO(II) chelate exposure were a higher decrease in cell density, cellular shrinkage, membrane blebbing, echinoid spikes, and the presence of apoptotic bodies.

Epidermal growth factor receptor (EGFR) plays an important role in epithelial malignancies and its activity can promote tumor growth, invasion and metastasis.[84] In normal tissues, the availability of EGFR ligands is tightly regulated to ensure that the kinetics of cell proliferation fully obey the rules of tissue homeostasis. However, in the case of cancer, EGFR is often persistent due to the continuous production of EGFR ligands in the tumor microenvironment. Therefore, the inhibition of the great growth of EGFR can play a role in cancer cell killing. Molecular docking was performed to point out the active amino acids participating in the interaction with the synthesized compounds and the potential of our compounds to retard the fast and great proliferation. It was found that both compounds, the ligand and its VO(II) chelate, exhibited scoring energies with negative signs that indicate a high stability of the compound-protein complex formation and consequently reveal the more favored interactions. The scoring energy values are −5.32 and −9.77 kcal mol^{-1} with 2.34 and 2.41 root mean square deviation (RMSD), respectively, which revealed the great affinity of the chelate relative to its parent (AA) ligand as an inhibitor for protein growth and consequently cancer denaturation.[85,86] As seen in Fig. 9, the Lys-*721* amino acid interacts with both the AA ligand and its VO(II) chelate through

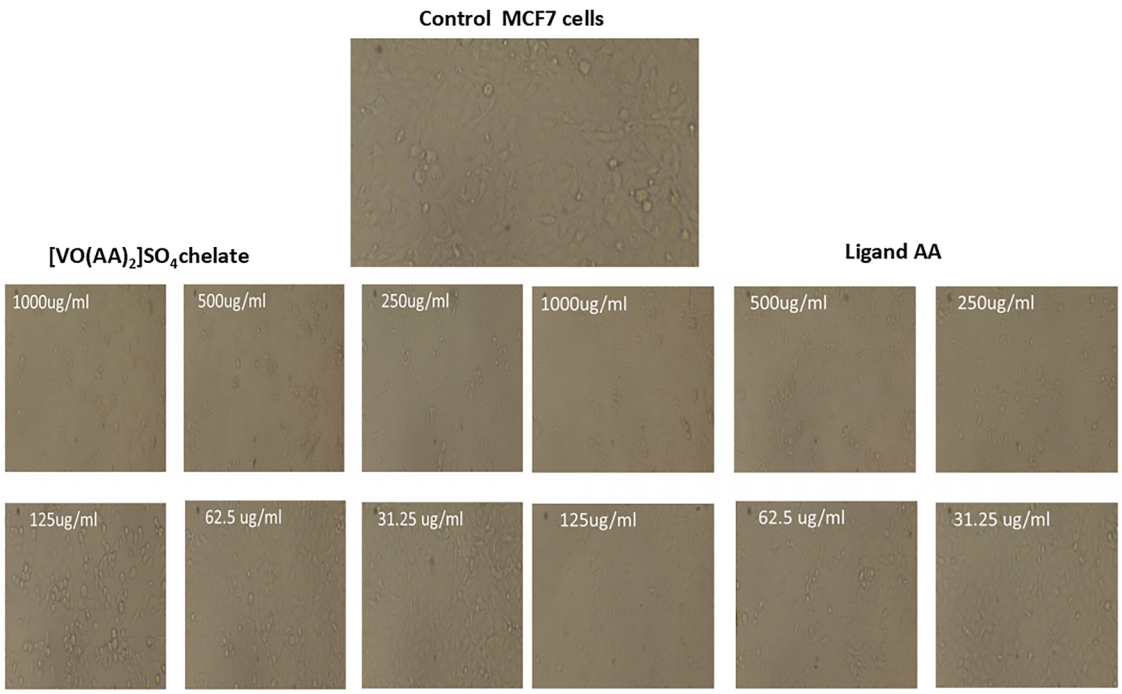

Fig. 8 Morphological change of (AA &$[VO(AA)_2]SO_4$) treated MCF-7 cells under an inverted microscope. Photos were taken at 60× magnification.

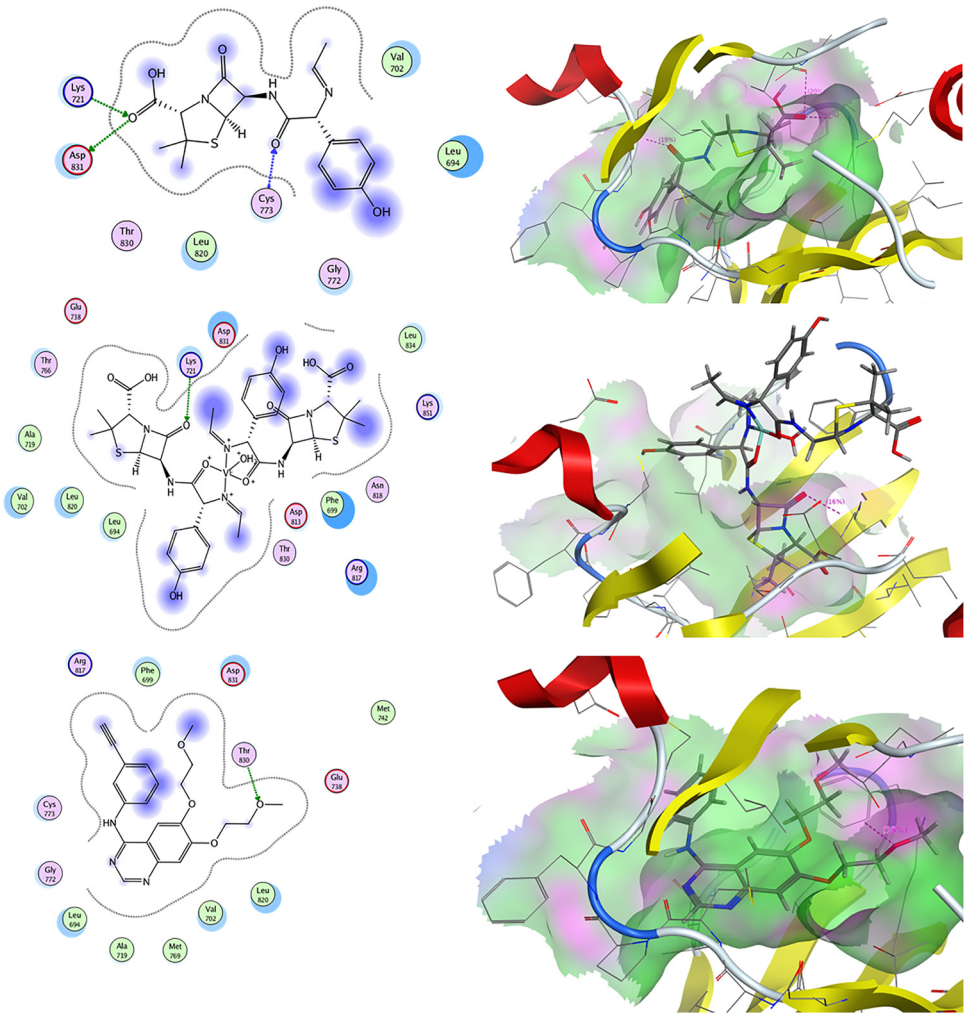

Fig. 9 2D and 3D crystal structure of interactions of the synthesized ligand, $[VO(AA)_2]SO_4$ chelate and AQ4 with amino acid residues in the binding site of the EGFR tyrosine kinase receptor (PDB Code: 1M17).

the sidechain donor, while the Cys-*773* amino acid interacts through the backbone donor and Asp-*831* through the side-chain acceptor in the case of the AA ligand. The different types of carbonyl groups of the amoxicillin drug are the active functional groups for hydrogen bond formation. To validate the docking protocol, the co-crystallized ligand AQ4 from the EGFR tyrosine kinase receptor (PDB ID: 1M17) was redocked into its original binding site. The redocking process yielded a binding energy of -4.28 kcal mol^{-1} and an RMSD of 2.8 Å, indicating acceptable accuracy. Notably, AQ4 maintained a key interaction with residue Thr-830, supporting the reliability of the docking method as shown in Fig. 9.

Inhibition of migration/wound healing of MCF-7 cells

The migration of MCF-7 cells in response to treatment with $[VO(AA)_2]SO_4$ was investigated by a wound healing assay. Overall, the results of the experiment in Fig. 10 reveal that MCF-7 cell migration was inhibited when treated with $[VO(AA)_2]SO_4$. At a concentration of 93.64 μg mL^{-1}, the MCF-7 cancer cell migration was suppressed by 46 039 mm over the untreated control at 48 h. These findings confirm that $[VO(AA)_2]SO_4$ has potential anti-cancer effects on MCF-7 cells. Furthermore, it was anticipated that the $[VO(AA)_2]SO_4$ would assist in reducing the metastasis of the studied cancer cells.

Effect of the compounds on DNA binding and denaturation inhibition of proteins

The affinity of drug binding to CT-DNA was assessed by tracking changes in both electrophoresis mobility and the intensity of the bands in an agarose gel using varying doses (5, 10, 15 μg mL^{-1}) of the investigated $[VO(AA)_2]SO_4$ complex and AA ligand. Fig. 11 displays the results of attaching the tested AA ligand and $[VO(AA)_2]SO_4$ complex in relation to the free, unbound CT-DNA, which causes a change in band intensity and migration of CT-DNA. A decrease in the total charge and an increase in the molecular mass of the CT-DNA due to interaction with the tested medication and/or a change in the structural conformation of the CT-DNA due to drug binding may be the reason for the DNA's decreased electrophoretic mobility.[87] These results are good and agree with other previous results of compounds based

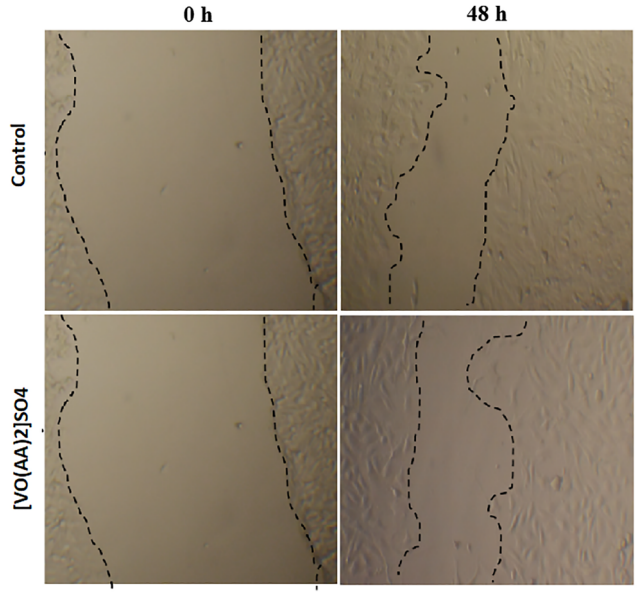

Fig. 10 The $[VO(AA)_2]SO_4$ effect on MCF-7 cell migration. The effect of MCF-7 cells after $[VO(AA)_2]SO_4$ exposure at 93.64 μg mL^{-1} concentration for 48 h using an inverted microscope at 10× magnification.

on the amoxicillin Schiff base.[88] One of the three primary causes of the decrease in band intensity seen in Fig. 11 as the concentration of each of the tested compounds increases is the covalent binding of the compound to CT-DNA, which damages certain regions of the DNA and reduces the amount of DNA available for ethidium bromide (EB) staining. DNA length was shown to affect the visible intensity of the stained DNA by ethidium bromide intercalation.[89] The second is the steric effect, which is brought on by the DNA attaching to a VO-containing medication, which reduces the DNA's availability for ethidium bromide intercalations.

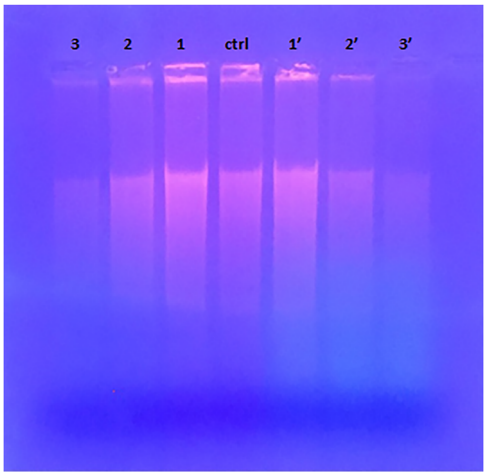

Fig. 11 DNA gel electrophoresis of CT-DNA bound to AA and $[VO(AA)_2]SO_4$ showing different migration and band intensity in comparison to the unbound CT-DNA, where lane ctrl is the unbound CT-DNA (20 μg mL^{-1}), while lanes 1, 2, and 3 are CT-DNA bound to the tested AA at 5, 10, and 15 μg mL^{-1}, respectively, and lanes 1′, 2′ and 3′ are the bound complex $[VO(AA)_2]SO_4$ at 5, 10, and 15 μg mL^{-1} of the complex, respectively.

The drug's planar aromatic moiety intercalates into neighboring DNA pairs, which is the third explanation. This would prevent EB from binding to CT-DNA in a competitive manner. Band intensities were quantified using ImageJ software to ensure objective measurement and to calculate the extent of binding. Densitometric analysis revealed a concentration-dependent reduction in DNA band intensity, supporting the formation of a stable complex between the compound and DNA.[90,91] The relative band intensity value was calculated for each concentration. The values for the AA ligand and its VO(II) chelate are (0.503, 0.147 & 0.133) and (0.815, 0.074 & 0.056) at concentrations (5, 10, & 15 μg mL^{-1})/compound.

Non-steroidal anti-inflammatory medications reduce inflammation by preventing protein denaturation, preventing enzyme hydrolysis, or encouraging membrane stability. In general, inflammation is brought on by either protein denaturation, as in arthritis, or lysosomal enzymes secreted by leukocytes.[92] In order to conduct additional pharmacological and biological testing, the prepared compounds were tested for their ability to inhibit protein denaturation. Both compounds can prevent protein denaturation in a manner that is dependent on the concentration. Protein denaturation increased with concentration for both the AA ligand and its VO(II) chelate. The AA ligand showed denaturation percentages of 0%, 7.5%, 25%, 42%, and 55% at 0, 5, 10, 20, and 30 μg mL^{-1}, respectively. In comparison, the VO(II) complex induced 0%, 9%, 29%, 45%, and 65% denaturation at the same concentration. The higher values observed for the VO(II) chelate suggest that metal coordination enhances the ability to disrupt the protein structure. The test makes the drug's anti-inflammatory action easier to grasp, even if additional research is required to fully understand and validate it.

Antidiabetic activity

Alpha-amylase inhibition with molecular docking investigation. In the present study, the synthesized compounds were screened for their inhibition activity against α-amylase. Fig. 12 depicts the inhibitory potency of the AA ligand and VO(II) chelate on α-amylase activity compared to a positive control (acarbose). The enzymatic activity of α-amylase progressively diminished with increasing concentrations of the produced AA, VO(II) chelate, and acarbose, achieving maximal inhibitions of 89.9%, 82.8%, and 98.0%, respectively. The half-maximal inhibitory concentration (IC_{50}) was utilized to compare the inhibitory capacities of our substances. A reduced IC_{50} value indicates an enhanced inhibitory action relative to the control. Both compounds have a significant effect that can be used as a good inhibitor of pancreatic α-amylase. The free Schiff base ligand exhibited superior α-amylase inhibitory activity compared to its VO(II) complex, with IC_{50} values of 48.86 ± 0.58 and 94.96 ± 1.65 μg mL^{-1}, respectively. This reduced activity upon metal coordination may be attributed to steric hindrance or diminished hydrogen-bonding interactions at the enzyme's active site, resulting from conformational changes or coordination of key functional groups. The lower α-amylase inhibitory activity of amoxicillin-based compounds compared to acarbose (IC_{50} = 6.84 ± 0.15 μg mL^{-1}) is likely due to their lack of

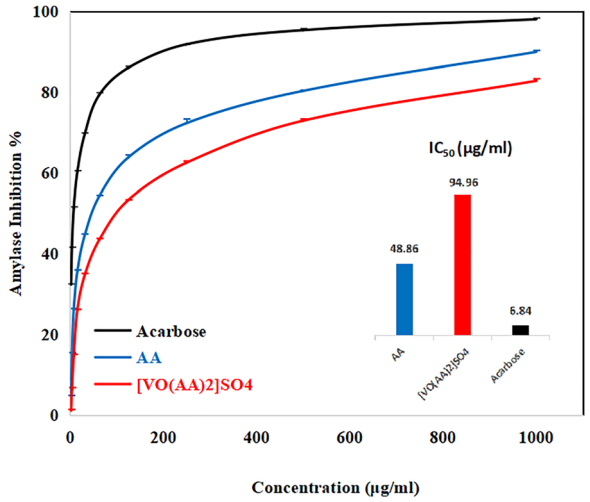

Fig. 12 Inhibitory effects of various concentrations of all compounds on α-amylase.

sugar-like features needed for strong enzyme binding, while acarbose is designed for this target. Raj Kaushal *et al.*[93] reported the IC_{50} value of various VO(II) complexes based on chalcone nuclei. The ligands and complexes revealed IC_{50} values in the range of 164.06–707.59 µg mL^{-1}. These values are significantly higher than those of our investigated compounds, showing that the amoxicillin-based compounds were effective inhibitors. Therefore, we can say that the amoxicillin nuclei succeeded in being a potent hypoglycemic agent. The synthesized compounds also exhibited potent activity compared to different reported natural compounds, such as gallic acid, *p*-coumaric acid, syringic acid, 2,3,4-trihydroxybenzoic acid, vanillic acid, caffeic acid and chlorogenic acid against porcine pancreatic α-amylase.[94] Therefore, we can say that the amoxicillin nuclei have a promising effect in the area of diabetes treatment. The inhibition role was indicated due to the hydrogen bond formation between the synthesized compounds and the enzyme, as seen in Fig. 13. The molecular docking revealed six and eight potential binding poses of the

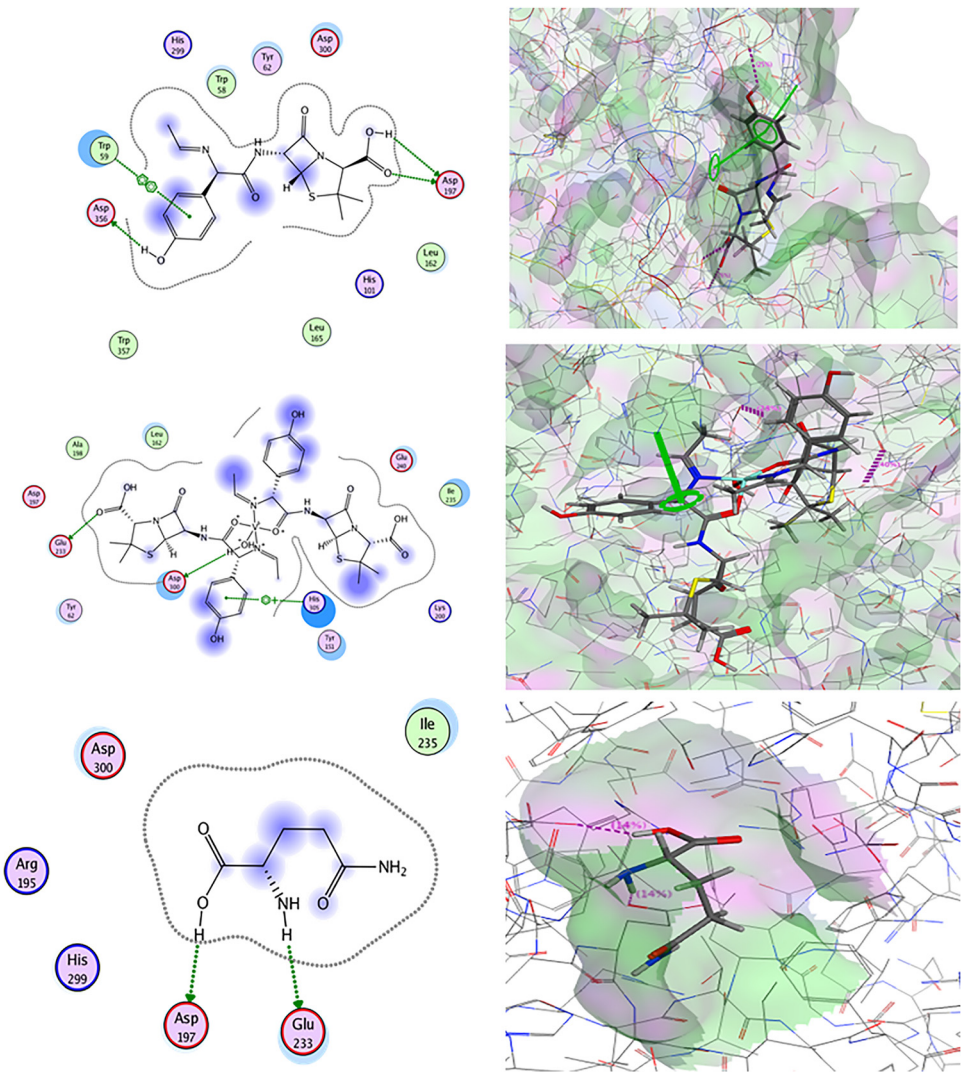

Fig. 13 A three-dimensional image of the binding of the ligand, $[VO(AA)_2]SO_4$ chelate and glutamine to the active site of α-amylase.

ligand and VO(II) chelate on α-amylase, respectively. The most probable binding site was determined to be the position at the active site with the highest absolute binding energy and the lowest root mean square deviation (RMSD). The ligand revealed (−6.56 kcal mol^{-1}, 1.34) and its VO (II) chelate (−10.95 kcal mol^{-1}, 2.31). The observed negative scoring energy sign indicates the high affinity of the interactions with the amylase enzyme. Fig. 13 depicts the 2D and 3D docking sites. The active site of α-amylase includes three active sites. The amino acids that participate in the interactions are (Asp-*356*, Asp-*197* & Glu-*233*), Trp-*59* and His-*305* with sidechain acceptor, arene–arene and arene–cation interactions, respectively. The docking method was checked by redocking the co-crystallized ligand glutamine into the active site of α-amylase (PDB ID: 1PIF). It gave a binding energy of −2.07 kcal mol^{-1} and an RMSD of 1.22 Å, showing good accuracy and important interactions with Glu-233 and Asp-197 as seen in Fig. 13.

Conclusion

New compounds derived from amoxicillin are synthesized through Schiff base formation using acetaldehyde and its VO(II) chelate. Both compounds are precisely characterized. The geometric arrangement of both compounds was confirmed *via* DFT analysis. The novel compounds evaluated for their effectiveness against breast cancer and diabetes demonstrate the dual action of amoxicillin on these two conditions. The amoxicillin derivative compounds were able to provide effective treatment for both breast cancer and diabetes. An investigation of DNA binding was conducted to verify the strong affinity of the compounds for DNA fragments, often proving effective as an anticancer agent. The compounds investigated showed significant impact as anti-inflammatory medications that demonstrate additional effects during cancer therapy. They not only served as a binding agent to DNA and slowed its rapid growth, but also assisted in addressing any inflammation caused during cancer development. In conclusion, we can state that the amoxicillin nuclei effectively aided in the treatment of two of the most severe diseases globally after being modified to VO(II) chelate and Schiff base through a straightforward method.

Author contributions

The authors have contributed equally to this work.

Conflicts of interest

The authors declare that they have no known competing financial interests or personal relationships that could have appeared to influence the work reported in this paper.

Data availability

The datasets used and analyzed during the current study are available from the corresponding author upon reasonable request. The data supporting this article have been included as part of the supplementary information (SI). Supplementary information is available. See DOI: **https://doi.org/10.1039/d5ma00567a**.

Acknowledgements

This work was funded by the University of Jeddah, Jeddah, Saudi Arabia, under grant no. (UJ-24-DR-1450-1). Therefore, the authors thank the University of Jeddah for its technical and financial support.

References

1 J. Ferlay, M. Ervik, F. Lam, M. Laversanne, M. Colombet, L. Mery, M. Piñeros, A. Znaor, I. Soerjomataram and F. Bray. Global cancer observatory: cancer today (version 1.1). Lyon, France: International Agency for Research on Cancer, 2024, **https://gco.iarc.who.int/today**.

2 H. Sung, J. Ferlay, R. L. Siegel, M. Laversanne, I. Soerjomataram, A. Jemal and F. Bray, Global cancer statistics 2020: GLOBOCAN estimates of incidence and mortality worldwide for 36 cancers in 185 countries, *CA-Cancer J. Clin.*, 2021, **71**, 209–249.

3 S. M. Afify and M. Seno, *Methods in Cancer Stem Cell Biology*, Springer, 2023.

4 F. Lordick and U. Hacker. Chemotherapy and Targeted Therapy, *Imaging of Complications and Toxicity following Tumor Therapy*, 2015, pp. 3–15.

5 L. Naso, M. Valcarcel, P. Villacé, M. Roura-Ferrer, C. Salado, E. G. Ferrer and P. A. M. Williams, Specific antitumor activities of natural and oxovanadium(IV) complexed flavonoids in human breast cancer cells., *New J. Chem.*, 2014, **38**, 2414–2421.

6 J. Barrios-González and A. Mejýa, Production of antibiotics and other commercially valuable secondary metabolites, *Current developments in solid-state fermentation*, Springer, New York, 2008, pp. 302–336.

7 Y. Gao, Q. Shang, W. Li, W. Guo, A. Stojadinovic, C. Mannion, Y.-G. Man and T. Chen, Antibiotics for cancer treatment: A double-edged sword, *J. Cancer*, 2020, **11**(17), 5135.

8 D. Yin and B. Yin, Influence of MP infection on immunologic function in patients with chronic obstructive pulmonary disease, *Hunan Yi Ke Da Xue Xue Bao*, 1998, **23**(5), 479–482.

9 L. S. Ashoor, I. K. Mohaisen and R. K. R. Al-Shemary, A review on versatile applications of transition metal complexes incorporating Schiff bases from amoxicillin and cephalexin, *EurAsian J. BioSci.*, 2020, **14**(2), 7541–7550.

10 M. S. Al-Rawi, D. F. Hussei, A. F. Al-Taie, M. M. Al-Halbosiy and B. A. Hameed, Cytotoxic effects of new synthesis heterocyclic derivatives of Amoxicillin on some cancer cell lines, *J. Phys.: Conf. Ser.*, 2018, **1003**, 012012.

11 A. Banerjee, M. Dahiya, M. T. Anand and S. Kumar, Inhibition of proliferation of cervical and leukemic cancer cells by penicillin G, *Asian Pac. J. Cancer Prev.*, 2013, **14**(3), 2127–2130.
12 N. Polyakov, T. Leshina, L. Fedenok, I. Slepneva, I. Kirilyuk, J. Furso and M. Olchawa, *et al.*, Redox-active quinone chelators: properties, mechanisms of action, cell delivery, and cell toxicity., *Antioxid. Redox Signaling*, 2018, **28**(15), 1394–1403.
13 A. R. White, C. Kaye, J. Poupard, R. Pypstra, G. Woodnutt and B. Wynne, Augmentin®(amoxicillin/clavulanate) in the treatment of community-acquired respiratory tract infection: a review of the continuing development of an innovative antimicrobial agent., *J. Antimicrob. Chemother.*, 2004, **53**(1), i3–i20.
14 M. S. Al-Rawi, D. F. Hussei, A. F. Al-Taie, M. M. Al-Halbosiy and B. A. Hameed, Cytotoxic effects of new synthesis heterocyclic derivatives of Amoxicillin on some cancer cell lines. In, *J. Phys.: Conf. Ser.*, 2018, **1003**(1), 012012.
15 U. Ndagi, N. Mhlongo and M. E. Soliman, Metal complexes in cancer therapy – an update from drug design perspective, *Drug Des., Dev. Ther.*, 2017, **11**, 599–616, DOI: **10.2147/DDDT.S119488**.
16 A. M. Evangelou, Vanadium in cancer treatment, *Crit. Rev. Oncol. Hematol.*, 2002, **42**(3), 249–265, DOI: **10.1016/S1040-8428(01)00202-7**.
17 P. Sharma, A. B. Jha and S. P. Singh, Repurposing antibiotics: Roles of metal complexes in antimicrobial and anticancer therapies, *Inorg. Chim. Acta*, 2021, **522**, 120376, DOI: **10.1016/j.ica.2021.120376**.
18 K. Choroba, B. Filipe, A. Switlicka, M. Penkala, B. Machura, A. Bienko, S. Cordeiro, P. V. Baptista and A. R. Fernandes, *In vitro* and *in vivo* biological activities of dipicolinate oxovanadium(IV) complexes., *J. Med. Chem.*, 2023, **66**(13), 8580–8599.
19 M. Turtoi, M. Anghelache, A. A. Patrascu, M. Deleanu, G. Voicu, M. Raduca, F. Safciuc, I. Manduteanu, M. Calin and D.-L. Popescu, Antitumor Properties of a New Macrocyclic Tetranuclear Oxidovanadium(v) Complex with 3-Methoxysalicylidenvaline Ligand., *Biomedicines*, 2022, **10**(6), 1217.
20 S. S. Hassan, D. H. Hanna and Sh. S. Medany, The double-edged sword of the amoxicillin antibiotic against prostate cancer in nano palladium form and its electrochemical detection of dopamine., *Appl. Organomet. Chem.*, 2023, **37**(4), e7026.
21 C. E. Heyliger, A. G. Tahiliani and J. H. McNeill, Effect of vanadate on elevated blood glucose and depressed cardiac performance of diabetic rats, *Science*, 1985, **227**, 1474–1477.
22 I. Goldwaser, D. Gefel, E. Gershonov, M. Fridkin and Y. Shechter, Insulin-like effects of vanadium: basic and clinical implications, *J. Inorg. Biochem.*, 2000, **80**, 21–25.
23 K. H. Thompson and C. Orvig, Metal complexes in medicinal chemistry: new vistas and recent advances, *Chem. Rev.*, 2009, **109**, 4185–4204.
24 A. B. Goldfine, D. C. Simonson, F. Folli, M. E. Patti and C. R. Kahn, Metabolic effects of vanadyl sulfate in humans with non-insulin-dependent diabetes mellitus: *in vivo* and *in vitro* studies, *Metabolism*, 2000, **49**(3), 400–410.
25 K. H. Thompson and C. Orvig, Vanadium in diabetes: 100 years from Phase 0 to Phase I, *J. Inorg. Biochem.*, 2006, **100**(12), 1925–1935.
26 A. K. Srivastava and M. Z. Mehdi, Insulino-mimetic and anti-diabetic effects of vanadium compounds, *Diabetic Med.*, 2005, **22**(1), 2–13.
27 D. Sanna, A. Fadda and M. Casula, *et al.*, Antidiabetic potential of vanadium complexes combined with olive leaf extracts: a viable approach to reduce metal toxicity, *Biometals*, 2025, **38**, 683–698.
28 L. H. Delgado-Rangel, V. Reyes-Márquez, M. E. Moreno-Narváez, A. Aragón-Muriel, J. R. Parra-Unda, J. A. Cruz-Navarro, M. A. Martínez-Torres, H. Valdés and D. Morales-Morales, Biological activity of vanadium pincer complexes., *New J. Chem.*, 2025, **49**, 3442–3455.
29 H. M. Alamri, A. I. Al-Sulami, M. Binkadem, M. T. Al-Sulami, S. A. Aly, S. S. Hassan, F. B. Rashidi, N. Terenti and E. M. Abdalla, Liver, Breast and Colon Anticancer, DNA Binding and Antimigration Investigation of Mono-and Binuclear Metal Complexes with Theoretical Studies, *Sci. Afr.*, 2025, **30**, e02991.
30 A. A. Van de Loosdrecht, R. H. J. Beelen, G. J. Ossenkoppele, M. G. Broekhoven and M. M. A. C. Langenhuijsen, A tetrazolium-based colorimetric MTT assay to quantitate human monocyte mediated cytotoxicity against leukemic cells from cell lines and patients with acute myeloid leukemia., *J. Immunol. Methods*, 1994, **174**, 311–320.
31 M. N. Wickramaratne, J. C. Punchihewa and D. B. M. Wickramaratne, In-vitro alpha amylase inhibitory activity of the leaf extracts of Adenanthera pavonina., *BMC Complementary Altern. Med.*, 2016, **16**, 1–5.
32 S. S. Hassan, W. M. Hosny, M. A. Aboutabl, D. B. Fayed and P. A. Khalf-Alla, Comparison of *In Vitro* and *In Vivo* Biological Screening of Nano-Palladium(II) and Platinum(II)-Based Compounds With DFT and Molecular Docking Study., *Appl. Organomet. Chem.*, 2024, **38**(12), e7713.
33 M. Frisch and F. Clemente, *Gaussian 09, revision a. 01*, 2009, 20–44.
34 H. A. Kyhoiesh and H. M. Hassan, Synthesis, characterization, in silico DFT, molecular docking, ADMET profiling studies and toxicity predictions of Ag(I) complex derived from 4-aminoacetophenone., *ChemistrySelect*, 2024, **9**(4), e202304429, DOI: **10.1002/slct.202304429**.
35 H. A. Kyhoiesh and Kh. J. Al-Adilee, Pt(IV) and Au(III) complexes with tridentate-benzothiazole based ligand: synthesis, characterization, biological applications (antibacterial, antifungal, antioxidant, anticancer and molecular docking) and DFT calculation., *Inorg. Chim. Acta*, 2023, **555**, 121598, DOI: **10.1016/j.ica.2023.121598**.
36 W. A. Al-Otaibi, S. M. Al Motwaa, A. S. Abubakr, S. S. Hassan and F. B. Rashidi, Targeted Colon Cancer and Chemotherapeutic Through Metal Glycoconjugates: Design, Synthesis, Molecular Docking, and DFT Investigations., *Appl. Organomet. Chem.*, 2025, **39**(3), e70000.

37 S. A. BenGuzzi, A. S. Abubakr and S. S. Hassan, Structural and biological studies of mononuclear metal(II) complexes containing hetero ligand based on 3-acetylpyridine thiosemicarbazone., *Appl. Organomet. Chem.*, 2023, **37**(9), e7203.
38 M. Morsy, S. S. Hassan, H. M. Shaker and K. M. Ismail, Synthesis and characterization of MIL-88B (Fe) MOF for high-performance humidity sensing, *Sens. Actuators, B*, 2025, **438**, 137806.
39 S. S. Hassan, E. F. Mohamed, K. Maged, S. Hassan, A. O. Hamad, S. Nasr and S. Reda, Synthesis of new Cu(II), Ni(II), and Cd(II)-(*N*-Glycyl-L-leucine) complexes as peptide metalloantibiotics for targeting pathogenic water with antioxidant effect investigation, *Beni-Suef Univ. J. Basic Appl. Sci.*, 2025, **14**(1), 46.
40 C. Bisson-Boutelliez, S. Fontanay, C. Finance and F. Kedzierewicz, Preparation and physicochemical characterization of amoxicillin β-cyclodextrin complexes, *AAPS PharmSciTech*, 2010, **11**, 574–581.
41 R. Di Stefano, M. Scopelliti, C. Pellerito, T. Fiore, R. Vitturi, M. S. Colomba, P. Gianguzza, G. C. Stocco, M. Consiglio and L. Pellerito, Organometallic complexes with biological molecules: XVII. Triorganotin(IV) complexes with amoxicillin and ampicillin., *J. Inorg. Biochem.*, 2002, **89**(3), 279–292.
42 G. B. Fogazzi, M. Cantu, L. Saglimbeni and M. Daudon, Amoxycillin, a rare but possible cause of crystalluria, *Nephrol., Dial., Transplant.*, 2003, **18**(1), 212–214.
43 H. K. Khassaf and W. A. Almasoudi, Pharmacological study of Schiff base derived from amoxicillin drug and vanillin, *J. Global Pharma Technol.*, 2009, **12**(6), 272–276.
44 V. U. Pawar and S. Joshi, Synthesis, characterization and biological studies of Schiff bases metal complexes Co(II), Zn(II), Ni(II), and Mn(II) derived from amoxicillin trihydrate with various aldehydes, *Int. J. Pharm. Bio. Sci.*, 2011, **2**, 240–250.
45 W. Al-Masoudi, H. Mohammad and A. Hama, Synthesis, characterization and pharmacological study of new Schiff base derived from amoxicillin drug, *Int. Res. J. Pharm.*, 2015, **6**, 386–389.
46 J. T. P. Matshwele, F. Nareetsile, D. Mapolelo, P. Matshameko, M. Leteane, D. O. Nkwe and S. Odisitse, Synthesis of Mixed Ligand Ruthenium (II/III) Complexes and Their Antibacterial Evaluation on Drug-Resistant Bacterial Organisms, *J. Chem.*, 2020, **2020**(1), 2150419.
47 M. Kaur and R. Kaushal, Synthesis, characterization and α-amylase and α-glucosidase inhibition studies of novel vanadyl chalcone complexes., *Appl. Organomet. Chem.*, 2021, **35**(1), e6042.
48 S. S. Hassan, N. M. H. Rizk, M. A. Khidr and S. A. Aly, Antibacterial, antifungal, and anticancer screening of some nano mono Co(II), Zn(II), Ru(III), and Ag(I) binuclear metal complexes of new hydrazone ligand., *Appl. Organomet. Chem.*, 2024, **38**(1), e7298.
49 S. S. Hassan, S. A. Aly, A. I. Al-Sulami, S. A. H. Albohy, M. F. Salem, G. M. Nasr and E. M. Abdalla, Synthesis, characterization, PXRD studies, and theoretical calculation of the effect of gamma irradiation and antimicrobial studies on novel Pd(II), Cu(II), and Cu(I) complexes, *Front. Chem.*, 2024, **12**, 1357330.
50 H. K. Khassaf and W. A. Almasoudi, Pharmacological study of Schiff base derived from amoxicillin drug and vanillin, *J. Global Pharma Technol.*, 2009, **12**(6), 272–276.
51 R. K. Mohapatra, P. K. Das, M. M. El-ajaily, U. Mishra and D. C. Dash, Synthesis, spectral, thermal, kinetic and antibacterial studies of transition metal complexes with benzimidazolyl-2-hydrazones of *o*-hydroxyacetophenone, *o*-hydroxybenzophenone and *o*-vanillin, *Bull. Chem. Soc. Ethiop.*, 2018, **32**(3), 437–450.
52 G.-B. Cao, Synthesis, characterization, and crystal structure of a novel trinuclear Schiff base Nickel(II) complex, *Synth. React. Inorg., Met.-Org., Nano-Met. Chem.*, 2007, **37**(8), 639–642.
53 S. S. Hassan, W. M. Hosny, M. A. Aboutabl, D. B. Fayed and P. A. Khalf-Alla, Comparison of *In Vitro* and *In Vivo* Biological Screening of Nano-Palladium(II) and Platinum(II)-Based Compounds With DFT and Molecular Docking Study, *Appl. Organomet. Chem.*, 2024, **38**(12), e7713.
54 K. M. Ismail, S. S. Hassan, S. S. Medany and M. A. Hefnawy, A novel Ni-complex nanocatalyst for efficient electrochemical oxidation of alcohol in alkaline medium: Mechanism and DFT study, *Electrochim. Acta*, 2024, **504**, 144954.
55 S. H. El-Taweel, S. S. Hassan and K. M. Ismail, Eco-friendly zinc-metal-organic framework as a nucleating agent for poly(lactic acid), *Int. J. Biol. Macromol.*, 2024, **271**, 132691.
56 M. A. Sultan, S. S. Hassan, K. A. Omran and H. B. Hassan, A novel Ni–Schiff base complex for motivating glucose electrooxidation in alkaline solutions, *Mater. Adv.*, 2024, **5**(3), 1264–1283.
57 H. A. El-Boraey, H. El-Ghnam, E. M. Atia and S. S. Hassan, Designing of some VO(II), Co(II) and Hg(II) Schiff base complexes: Synthesis, structure elucidation, anticancer and biopesticidal activities, DFT and docking approaches, *Results Chem.*, 2024, **11**, 101767.
58 W. Al-Masoudi, H. Mohammad and A. Hama, Synthesis, characterization and pharmacological study of new Schiff base derived from amoxicillin drug, *Int. Res. J. Pharm.*, 2015, **6**, 386–389.
59 L. M. Monleón, F. Díez-García, H. Zamora, J. Anaya, M. Grande, J. G. de Diego and F. D. Rodríguez, *In vitro* evaluation of the antielastase activity of polycyclic β-lactams., *Bioorg. Chem.*, 2012, **45**, 29–35.
60 K. Yao, N. Li and L. Shen, Synthesis and catalytic activity of Ln(III) complexes with an unsymmetrical Schiff base including multi groupsgroups., *Sci. China, Ser. B: Chem.*, 2003, **46**, 75–83.
61 L. K. Abdul Karem and T. H. Al-Noor, Mixed Ligand Complexes of Schiff Base and Nicotinamide: Synthesis, Characterization and Antimicrobial Activities, *J. Phys.: Conf. Ser.*, 1660, **1**(2020), 012094.
62 A. A. Diamantis and J. V. Dubrawski, Preparation and coordination geometry of quadridentate ethylenediaminetetraacetate complexes of ruthenium(II) and -(III)., *Inorg. Chem.*, 1983, **22**(13), 1934–1946.

63 T. Storr, B. R. Cameron, R. A. Gossage, H. Yee, R. T. Skerlj, M. C. Darkes and S. P. Fricker, *et al.*, Ru(III) complexes of edta and dtpa polyaminocarboxylate analogues and their use as nitric oxide scavengers, *Eur. J. Inorg. Chem.*, 2005, 2685–2697.

64 S. H. Mahdi, Spectroscopic, structural and antibacterial activity of mixed ligand complexes from Schiff base with anthranilic acid, *J. Phys.: Conf. Ser.*, 2019, **1234**(1), 012089.

65 A. Reiss, A. Samide, G. Ciobanu and I. Dabuleanu, Synthesis, spectral characterization and thermal behaviour of new metal(II) complexes with Schiff base derived from amoxicillin, *J. Chil. Chem. Soc.*, 2015, **60**(3), 3074–3079.

66 J. M. Mir, B. A. Malik, M. W. Khan and R. C. Maurya, A novel oxovanadium (IV) complex containing pyranone appended glucosamine Schiff base: synthesis, characterization and DFT evaluation, *J. Coord. Chem.*, 2020, **73**(20), 2906–2918.

67 M. R. Maurya, H. Singh and A. Pandey, Dioxovanadates(V) α Potassium bis (2-through) base assisted aerial oxidation of the corresponding oxovanadium(IV) complexes., *Synth. React. Inorg. Met.-Org. Chem.*, 2002, **32**, 231–242.

68 A. M. Naglah, Moamen S. Refat, M. A. Al-Omar, M. A. Bhat, H. M. AlKahtani and A. S. Al-Wasidi, Synthesis of a vanadyl(IV) folate complex for the treatment of diabetes: spectroscopic, structural, and biological characterization., *Drug Des., Dev. Ther.*, 2019, 1409–1420.

69 K. M. Ismail, S. S. Hassan and D. H. Hanna, Palladium-Imidazole Nanoparticles' Cytotoxic Effects on Colon Cancer Cells: Induction of Cell Cycle Arrest and Apoptosis Mediated *via* Mitochondria., *Appl. Organomet. Chem.*, 2025, **39**(1), e7908.

70 M. A. Sultan, H. B. Hassan, S. S. Hassan and K. M. Ismail, Enhanced electrocatalytic alcohol oxidation with Ni-MOF for direct alcohol fuel cell applications, *Int. J. Hydrogen Energy*, 2025, **100**, 528–547.

71 K. M. Ismail, F. B. Rashidi and S. S. Hassan, Ultrasonic synthesis, characterization, DFT and molecular docking of a biocompatible Zn-based MOF as a potential antimicrobial, anti-inflammatory and antitumor agent., *Sci. Rep.*, 2024, **14**(1), 21989.

72 C. Güleryüz, D. M. Hasan, M. A. Awad, A. S. Waheeb, A. U. Hassan, A. Mohyuddin, H. A. K. Kyhoiesh and M. T. Alotaibi, Molecular engineering on tyrian puprle natural dye as TiO_2 based fined tuned photovoltaic dye material: DFT molecular analysis., *J. Mol. Graphics Modell.*, 2025, **134**, 108894, DOI: **10.1016/j.jmgm.2024.108894**.

73 E. M. Abdalla, S. A. Aly, A. H. Salama, S. S. Hassan, A. M. Mongy, T. A. Salem and P. A. Khalf-Alla, Synthesis, Characterization, DFT, TEM, Anticancer, Antibacterial, and Electrical Properties Studies of Novel VO(II), Cu(II), Ru(III), and Ag(I) Complexes With Hydrazone Derivatives., *Appl. Organomet. Chem.*, 2025, **39**(3), e70073.

74 S. S. Hassan, S. A. Aly, R. A. Ismail, A. M. Aboelyazed, M. H. Youssef and E. M. Abdalla, Molecular Structure, Docking, Spectroscopic Characterization, Antibacterial, and Anticancer Activity of Copper(I,II), Silver(I), and Cadmium(II) Complexes, *Appl. Organomet. Chem.*, 2025, **39**(2), e7990.

75 J. P. Merrick, D. Moran and L. Radom, An evaluation of harmonic vibrational frequency scale factors, *J. Phys. Chem. A*, 2007, **111**(45), 11683–11700.

76 A. Bagno, F. Rastrelli and G. Saielli, Prediction of the ^{1}H and ^{13}C NMR spectra of α-D-glucose in water by DFT methods and MD simulations, *J. Org. Chem.*, 2007, **72**(19), 7373–7381.

77 M. Aureliano, A. Luísa De Sousa-Coelho, C. C. Dolan, D. A. Roess and D. C. Crans, Biological consequences of vanadium effects on formation of reactive oxygen species and lipid peroxidation, *Int. J. Mol. Sci.*, 2023, **24**(6), 5382.

78 J. Zou, L. Zhu, X. Jiang, Y. Wang, Y. Wang, X. Wang and B. Chen, Curcumin increases breast cancer cell sensitivity to cisplatin by decreasing FEN1 expression., *Oncotarget*, 2018, **9**(13), 11268.

79 L. Galluzzi, I. Vitale, J. Michels, C. Brenner, G. Szabadkai, A. Harel-Bellan, M. Castedo and G. J. C. D. Kroemer, Systems biology of cisplatin resistance: past, present and future, *Cell Death Dis.*, 2014, **5**(5), e1257.

80 X. J. Fang, H. Jiang, Y. Q. Zhu, L. Y. Zhang, Q. H. Fan and Y. Tian, Doxorubicin induces drug resistance and expression of the novel CD44st *via* NF-κB in human breast cancer MCF-7 cells., *Oncol. Rep.*, 2014, **31**(6), 2735–2742.

81 Amoxicillin – Drug Information. Drugs.com. Available at: **https://www.drugs.com/amoxicillin.html**.

82 S. S. Hassan, E. F. Mohamed, A. M. Saleh, M. M. Shoukry and P. A. Khalf-Alla, Design, structural characterization, DFT, molecular docking, and chemotherapeutic activity of novel platinum(II) and palladium(II) complexes derived from Metformin-based Schiff base, *J. Mol. Struct.*, 2024, **1315**, 138830.

83 S. S. Hassan, E. A. Bedir, A. M. Hamza, A. M. Ahmed, N. M. Ibrahim, M. S. Abd El-Ghany and N. N. Khattab, The dual therapeutic effect of metformin nuclei-based drugs modified with one of Tulbaghia violacea extract compounds, *Appl. Organomet. Chem.*, 2022, **36**(9), e6804.

84 H. Masuda, D. Zhang, C. Bartholomeusz, H. Doihara, G. N. Hortobagyi and N. T. Ueno, Role of epidermal growth factor receptor in breast cancer, *Breast Cancer Res. Treat.*, 2012, **136**(2), 331–345.

85 A. S. Waheeb, M. A. Awad, H. A. K. Kyhoiesh, A. M. Kadhum, J. A. Thabit and S. A. Lazam, Synthesis, and characterization of Ni(II), and Cu(II) metal complexes containing new azo dye ligand (N, N, N) and evaluation of their biological activities supported by DFT studies, molecular docking, ADMET profiling, drug-likeness analysis and toxicity prediction, *J. Mol. Struct.*, 2025, **1321**, 139867, DOI: **10.1016/j.molstruc.2024.139867**.

86 A. S. Waheeb and H. A. K. Kyhoiesh, Ni(II) and Cu(II) Complexes With a Tridentate (O, N, O) Azo Dye Antipyrine-Based Ligand: Synthesis, Spectral Characterization, Cytotoxicity, and In Silico Approaches, *Appl. Organomet. Chem.*, 2025, **39**(5), e70144, DOI: **10.1002/aoc.70144**.

87 H. Mansouri-Torshizi, S. Zareian-Jahromi, K. Abdi and M. Saeidifar, Nonionic but water soluble,[Glycine-Pd-Alanine] and [Glycine-Pd-Valine] complexes. Their synthesis,

characterization, antitumor activities and rich DNA/HSA interaction studies, *J. Biomol. Struct. Dyn.*, 2019, **37**, 3566–3582.

88 S. S. Hassan, M. Nader, M. Nagy, M. Mohamed, M. Nader, M. Zakaria, N. Mohamed, R. Waleed and F. B. Rashidi, Antimicrobial screening involving Helicobacter pylori of nano-therapeutic compounds based on the amoxicillin antibiotic drug, *Helicobacter*, 2023, **28**(5), e13004.

89 T. Thibault, J. Degrouard, P. Baril, C. Pichon, P. Midoux and J. Malinge, Production of DNA minicircles less than 250 base pairs through a novel concentrated DNA circularization assay enabling minicircle design with NF-κB inhibition activity, *Nucleic Acids Res.*, 2017, **45**(5), e26.

90 A. Ghatak, A. Das and S. Roy, Densitometric quantification of DNA damage in gel electrophoresis, *Methods Mol. Biol.*, 2013, **920**, 363–371, DOI: **10.1007/978-1-61779-998-3_28**.

91 G. Zhao, W. Guo, M. Wang and Y. Wang, DNA binding and cleavage studies of a novel copper(II) complex: experimental and theoretical studies, *J. Photochem. Photobiol., B*, 2014, **130**, 264–271, DOI: **10.1016/j.jphotobiol.2013.11.006**.

92 K. S. R. Gunathilake and H. P. V. Rupasinghe, *In vitro* anti-inflammatory properties of selected green leafy vegetables, *Biomedicines*, 2018, **6**(4), 107.

93 M. Kaur and R. Kaushal, Synthesis, characterization and α-amylase and α-glucosidase inhibition studies of novel vanadyl chalcone complexes, *Appl. Organomet. Chem.*, 2021, **35**(1), e6042.

94 Y. Huang, S. J. Richardson, C. S. Brennan and S. Kasapis, Mechanistic insights into α-amylase inhibition, binding affinity and structural changes upon interaction with gallic acid, *Food Hydrocolloids*, 2024, **148**, 109467.